water

MDPI

Article

Regionalisation of Generalised Extreme Value Distribution in Regional Flood Frequency Analysis: A Case Study for South-East Australia

Laura Rima [1], Khaled Haddad [1] and Ataur Rahman [2,*]

[1] School of Engineering, Building XB, Penrith Campus, Western Sydney University, Penrith, NSW 2747, Australia; l.rima2@westernsydney.edu.au (L.R.); k.haddad@westernsydney.edu.au (K.H.)
[2] Sustainability Engineering Discipline, School of Engineering, Western Sydney University, Penrith, NSW 2747, Australia
* Correspondence: a.rahman@westernsydney.edu.au

Abstract

This study presents regionalisation of the Generalised Extreme Value (GEV) distribution by adopting L moments and Bayesian Generalised Least Squares (BGLS) regression. This uses data from 88 gauged catchments in New South Wales, Australia. The regional GEV distribution is compared using the Parameter Regression Technique (PRT) and Quantile Regression Technique (QRT) under fixed-region and Region-of-Influence (ROI) approaches. Results indicate improved regional flood estimation, capturing spatial variability and reducing uncertainty in flood quantile estimation through the ROI approach compared to fixed regions. The mean flood statistic shows a higher spatial heterogeneity in the fixed region approach, while the ROI approach more effectively reduces uncertainty and enhances predictive performance. For fixed regions, PRT achieves a median relative error (Rer%) of 34–40% and a relative root mean square error (RRMSE%) of 59–65%, compared with QRT's Rer% of 40–63% and RRMSE of 59–94%. In the ROI framework, both techniques yield similar Rer% (31–40%), though QRT-ROI exhibits slightly reduced RRMSE.

Keywords: floods; RFFA; GEV; PRT; ROI; QRT; Australia

1. Introduction

Design flood estimation plays a critical role in water resources management by enabling robust flood risk assessments and the development of effective flood control measures for communities and infrastructure across diverse regions [1–3]. While on-site flood frequency analysis (FFA) remains the staple statistical approach for determining design floods at individual locations, its practical use is often limited by sparsity and insufficient length of flood records. To address these limitations, Regional Flood Frequency Analysis (RFFA) is widely adopted, allowing hydrologists to transfer flood data and insights from well-gauged sites to ungauged or data-deficient catchments within a defined region [4–6].

A major challenge in RFFA is ensuring the quality and reliability of streamflow records at gauged sites, while also accounting for changes in basin characteristics due to processes such as urbanisation and land use change (including forest reclamation), which can alter runoff generation and affect the adequacy of regional models [7–9]. Despite such issues, RFFA methodologies have been successfully implemented on national and international scales, including Australia, the United States, Europe, and Asia, and have contributed significantly to modern flood risk assessment [2,10–12]. These techniques encompass the Probabilistic Rational

Check for updates

Academic Editor: Christos S. Akratos

Received: 28 April 2026
Revised: 4 June 2026
Accepted: 13 June 2026
Published: 17 June 2026

Copyright: © 2026 by the authors. Licensee MDPI, Basel, Switzerland. This article is an open access article distributed under the terms and conditions of the Creative Commons Attribution (CC BY) license.

Method [13–15], the classic Index Flood Method [16–22], and more recent approaches such as generalised additive models [23–26] and artificial intelligence-based flood estimation [27–29].

A central foundation of RFFA is the use of regional regression techniques, most commonly the Quantile Regression Technique (QRT) and Parameter Regression Technique (PRT). QRT involves regressing observed flood quantiles against catchment characteristics and is preferred for its simplicity and ability to capture key physiographic and climate controls on flood behaviour [30,31]. In contrast, PRT involves regressing the parameters of a selected flood frequency distribution (typically mean, scale, and shape) against catchment variables, after which these parameters are used to estimate flood quantiles over a range of annual exceedance probabilities [8,32,33]. Flood design levels for 2, 5, 10, 20, 50, and 100 years (Q_2–Q_{100}) are typically targeted in such studies. Unique to PRT is its capacity to preserve smooth changes in annual exceedance probability (AEP)-quantile relationships, which can be important in engineering design [11].

Comparative research suggests that while QRT may sometimes yield more accurate predictions for lower AEPs, PRT tends to outperform QRT as the return period increases, especially under conditions of significant regional heterogeneity [32,34]. For instance, [8] demonstrated that PRT was both more accurate and computationally efficient than QRT for spatially proximate catchments in the northeastern United States, and [35] showed that paired with independent component analysis, PRT surpassed QRT in New South Wales, Australia. The selection of the optimal method should therefore consider both statistical performance and application context, as well as the availability and type of predictor variables.

Traditional OLS regression, though long employed in flood data modelling, is subject to strong assumptions including equal record lengths and independence of concurrent floods between stations—conditions rarely met in practice. This motivated the development of Generalised Least Squares (GLS) regression models, which explicitly account for inter-site correlation and differences in record lengths [11,12,36,37]. To further enhance accuracy, Bayesian Generalised Least Squares (BGLS) regression was introduced, enabling improved estimation of model error variance and greater control over predictive uncertainty through specification of prior distributions [12,38–40]. Work by [34] indicates that with proper implementation, BGLS can yield comparable performance for both QRT and PRT in regional settings.

Regionalisation in RFFA is typically achieved via fixed regions (e.g., administrative boundaries, physiographic zones) or more flexible approaches such as Region of Influence (ROI). Fixed regions offer simplicity but can lead to discontinuities or bias at boundaries, as regional flood equations may shift sharply at arbitrary divisions [33,41]. Ref. [42] pioneered non-fixed regions, while refs [43–45] formalised ROI where regions are dynamically defined based on hydrologic or geographic proximity among catchments. The ROI framework enables the creation of tailored subregions that respond better to local hydrologic conditions, often yielding higher predictive accuracy than fixed-region models, especially in heterogeneous environments such as Australia [34,46–48]. ROI is now the preferred procedure in national flood estimation guidelines, including Australian Rainfall and Runoff [49].

Uncertainty remains an important concern in RFFA, caused by data sampling, measurement error, inter-site correlation, and model complexity [38,50,51]. Advanced methods such as BGLS integrate and manage these uncertainties directly, yielding superior reliability for regional flood prediction.

The selection of the underlying flood frequency distribution is critical: although earlier Australian studies commonly used the Log-Pearson Type III (LP3) distribution [52,53], recent evidence supports the Generalised Extreme Value (GEV) distribution as a best performer for both flood and rainfall in a variety of settings [54–58]. The GEV's flexibility and robustness to outliers, especially when estimated using L-moments, make it ideal for regionalisation efforts, particularly where sample sizes are modest [58–60].

Australian RFFA literature highlights the need to further explore regionalisation of GEV parameters via L-moments within a BGLS framework. Previous studies have investigated BGLS, ROI, PRT, and QRT in Australian RFFA applications [34]; however, relatively limited research has provided a systematic comparison of QRT and PRT for GEV within a unified BGLS framework, particularly under both fixed-region and ROI approaches. By harnessing L-moments and Bayesian approaches, this research aims to further improve regional flood prediction methods for NSW catchments and provide insights that may be relevant to regions with comparable hydro-climatic characteristics. Therefore, this study develops RFFA prediction models for six AEPs (50%, 20%, 10%, 5%, 2%, and 1%) in New South Wales, Australia, by regionalising GEV parameters (mean, LCV, LSK) via PRT and directly predicting flood quantiles via QRT, both using BGLS regression methodology. Comparison is made between fixed region and ROI approaches using leave-one-out cross-validation and robust evaluation statistics. In addition, a sensitivity analysis is performed to assess the impact of prior information in BGLS regression. These GEV-BGLS-based RFFA models provide additional understanding of the relative performance of regionalisation approaches and may assist in improving flood quantile estimates for ungauged sites in NSW catchments.

2. Materials and Methods

2.1. Study Area and Data

New South Wales (NSW), Australia, was chosen for this study due to superior streamflow data quality compared to other Australian states, alongside an extensive database of long-term flood records. A total of 88 gauged catchments, classified as natural and small to medium-sized, were selected for regional analysis following the guidelines and prior research of [14]. Catchments were required to have a minimum streamflow record length of 25 years and a maximum catchment area of approximately 1000 km^2 to improve the reliability of flood quantile estimation. Only predominantly unregulated catchments with good quality AMF records and limited urbanisation were included to minimise the influence of flow regulation and significant hydrologic alteration on the regional analysis.

The catchment sizes range from 8 to 1010 km^2, with an average of approximately 325 km^2 and a median of 260 km^2. Annual maximum flood (AMF) records for these catchments span 25 to 89 years, averaging 48 years with a median of 44 years. The spatial distribution of the selected catchments is shown in Figure 1, providing coverage across hydro-climatic zones in the state. While these selection criteria improve the consistency and robustness of the developed regional models, the results may be less directly applicable to highly regulated or strongly modified catchments outside the analysed NSW dataset.



Figure 1. Location of the 88 catchments in NSW, Australia (shown as red dots).

2.2. Selection of Catchment Characteristics

Eight catchment characteristics were chosen as predictor variables to develop and validate the regional flood frequency analysis (RFFA) models. Table 1 presents summary statistics for each variable across the 88 selected catchments. Each variable was selected based on its hydrological relevance and precedence in regional studies:

- Catchment area (*Area*): controls the magnitude of flood peaks, with larger catchments typically producing higher flow events given similar conditions.
- Design rainfall intensity ($I_{6,2}$): represents six-hour rainfall at 1-in-2 AEP, obtained from Bureau of Meteorology grids at catchment centroids.
- Mean annual rainfall (*MAR*): acts as a proxy indicator for variables influencing flood generation, though not directly a determinant of peak flows.
- Shape factor (*SF*): describes catchment geometry, which influences runoff speed—elongated catchments generally respond more slowly than circular ones.
- Mean annual evapotranspiration (*MAE*): governs water loss via surface and atmospheric transfer, impacting runoff and groundwater recharge.
- Stream density (*SDEN*): the sum of stream lengths per area, reflecting drainage efficiency and potential for rapid runoff generation.
- Slope factor (*S1085*): the average channel slope over the central 75% of stream length, affecting velocity and timing of flood response.
- Forest cover (*FOREST*): fraction of catchment under forest, affecting infiltration, soil moisture, and ultimate flood volume.

Table 1. Summary of descriptive statistics of 88 catchment characteristics. Predictor variables are presented in italics.

Catchments Characteristics	Min	Max	Mean	Standard Deviation
Area (km^2)	8	1010	351.98	281.43
$I_{6,2}$ (mm)	31.40	88.50	45.36	11.21
MAR (mm/year)	626.17	1953.23	1000.28	304.48
SF	0.26	1.629	0.76	0.21
MAE (mm/year)	980.40	1543.30	1223.69	126.30
SDEN (mm/km^2)	0.52	5.474	2.85	1.099
S1085 (m/km)	1.54	49.86	12.92	10.80
FOREST (%)	0.010	0.990	0.51	0.32

These predictor variables were selected based on their demonstrated importance in Australian RFFA studies [34,35]. The selection was guided by hydrological significance, data availability, and the ability of the variables to represent key physical and climatic controls on flood generation. Alternative combinations of predictor variables were evaluated during model development, and the final predictor sets were selected based on both statistical performance and physical interpretability. Descriptive statistics across stations are as follows:

2.3. Data Transformation and Correlation Analysis

Initial correlation analysis among the eight catchment predictors revealed notable skewness and non-linear relationships, particularly in variables such as *Area*, $I_{6,2}$, and *FOREST*. To address this and to meet regression model assumptions, a log transformation was applied to all predictors when developing regression equations. Log transformation improved normality, reduced outlier impact, and enhanced linearity among variables, especially between *Area* and *MAR*. For increased interpretability of regression coefficients and to meet model selection criteria, all transformed variables were then centred on their means. Figures 2 and 3, respectively, depict raw and transformed correlations among predictors

that demonstrate substantial improvements in distribution and relationships after transformation, confirming suitability for use in subsequent Bayesian GLS regression analysis.

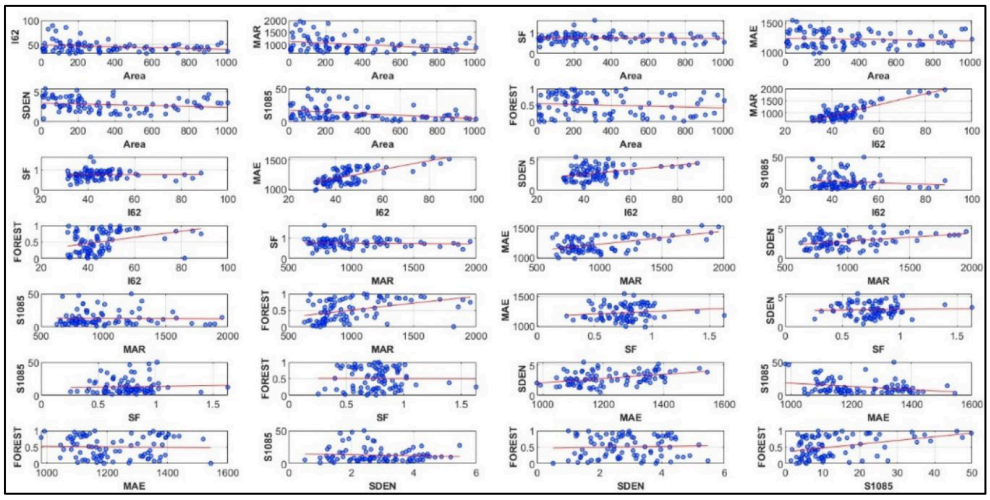


Figure 2. Correlations (raw) among the selected catchment characteristics. The red line represents the fitted linear trend line.

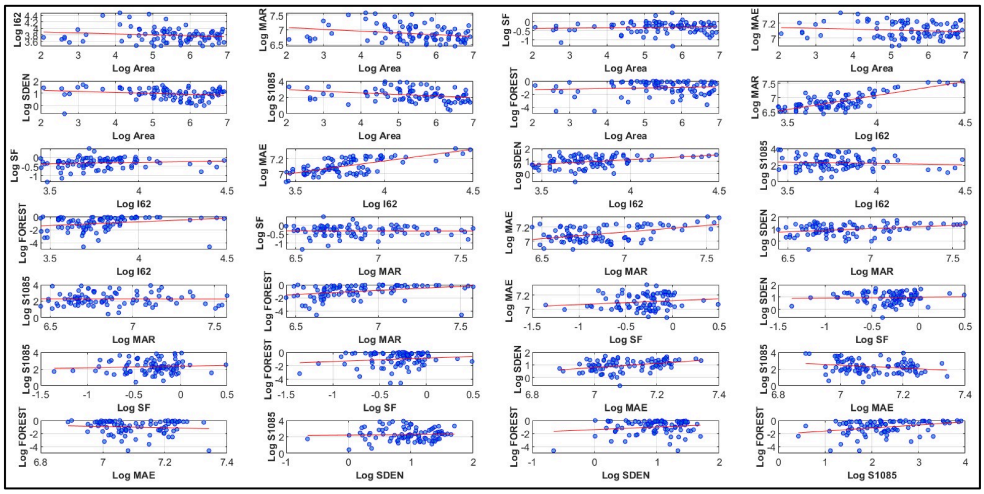


Figure 3. Correlations among log-transformed catchment characteristics. The red line represents the fitted linear trend line.

2.4. Methodology

2.4.1. Generalised Extreme Value (GEV) Distribution and L-Moments

At-site flood frequency analysis was performed using the Generalised Extreme Value (GEV) distribution implemented through FLIKE software (version 5.0.300.0; University of Newcastle, Newcastle, NSW, Australia) developed by [61,62]. For each catchment, the FLIKE software estimated the GEV location, scale, and shape parameters from the AMF series, from which the design flood quantiles (Q_2–Q_{100}) were derived.

Prior to selection of the GEV distribution, five candidate probability distributions including GEV, LP3, Lognormal, Gumbel, and Generalised Pareto were evaluated using multiple goodness-of-fit (GoF) measures including Anderson–Darling (AD), Kolmogorov–Smirnov (KS), Chi-square (CS), and Z^{DIST} tests together with L-moment ratio diagrams. Earlier GoF analysis undertaken on a larger eastern Australian dataset showed that the GEV distribution ranked first in 133 stations for the AD test, 157 stations for the KS test, and 156 stations for the CS test, demonstrating strong overall performance for modelling flood extremes.

The GEV distribution was selected based on its demonstrated effectiveness in Australian rainfall estimation within Australian Rainfall and Runoff guidelines [63], with the GoF assessment indicating that GEV provided satisfactory and stable performance for NSW annual maximum flood (AMF) data, particularly for higher flow extremes. The GEV distribution, originally proposed by [64], provides significant advantages over traditional distributions including superior flexibility [65] and resilience when managing low flows due to reduced outlier sensitivity [18,66]. The three-parameter GEV distribution is expressed as:

$$F_x(x) = exp\left\{-\left[1-\frac{\kappa(x-\mu)}{\alpha}\right]^{\frac{1}{\kappa}}\right\}, \quad for\ \kappa \neq 0 \tag{1}$$

where μ denotes location parameter, α scale parameter, and κ shape parameter. Flood quantiles were estimated for six AEPs being: 50%, 20%, 10%, 5%, 2%, and 1% AEPs, respectively.

L-moments provide substantial advantages over traditional moments through superior stability with limited sample sizes and resistance to outlier influence. Calculation requires Probability Weighted Moments (PWMs), with data arranged in ascending order using equations as shown below and in [67].

$$M_{100}= \mathrm{E[Q]},\ M_{110}= \mathrm{E}[QF(Q)],\ M_{120}= \mathrm{E}\left[QF(Q)^2\right],\ M_{130} = \mathrm{E}[QF)^3] \tag{2}$$

where Q denotes the annual maximum flow and $F(Q)$ is its cumulative distribution function. The first four L-moments (λ_1, λ_2, λ_3, λ_4) are linear combinations of these PWMs:

$$\lambda_1 = L_1 = M_{100} \tag{3}$$

$$\lambda_2 = L_2 = 2M_{110} - M_{100} \tag{4}$$

$$\lambda_3 = L_3 = 6M_{120} - 6M_{110} + M_{100} \tag{5}$$

$$\lambda_4 = L_4 = 20M_{130} - 30M_{120} + 12M_{110} - M_{100} \tag{6}$$

L-moment ratios include LCV (τ_2), L-Skewness (LSK) τ_3, and L-Kurtosis (LKurt) τ_4, defined by [68] as:

$$\mathrm{LCV} = \tau_2 = {}^{\lambda_2}/_{\lambda_1},\ \mathrm{LSK} = \tau_3 = {}^{\lambda_3}/_{\lambda_2},\ \mathrm{LKurt} = \tau_4 = {}^{\lambda_4}/_{\lambda_2} \tag{7}$$

GEV parameters (location μ, scale α and shape κ) are computed using [58] empirically derived formulae for LSK values (τ_3) between -0.5 and 0.5.

$$\kappa = 7.8590c + 2.9554c^2,\ \text{where } c = \frac{2}{3+|\tau_3|} - \frac{\ln 2}{\ln 3} \tag{8}$$

$$\alpha = \frac{\lambda_2\kappa}{(1-2^{-\kappa})\Gamma(1+k)},\ \mu = \lambda_1 - \alpha\frac{[1-\Gamma(1+\kappa)]}{\kappa}, \tag{9}$$

where Γ represents the gamma function.

T-year flood quantiles are then calculated using:

$$Q_T = \mu + \left(\frac{\alpha}{\kappa}\right)\left[1-\left(-\log\left(\frac{T-1}{T}\right)\right)^{\kappa}\right] \tag{10}$$

Log transformation was applied to all dependent variables except LCV and LSK to improve normality and linearity.

2.4.2. Generalised Least Squares (GLS) Regression Framework

GLS regression addresses fundamental assumptions often violated in hydrological data: equal record lengths and independence between concurrent floods [36,37]. The general regression model assumes hydrological variable y_i at station i:

$$y_i = \beta_0 + \sum_{j=1}^{k} \beta_j X_{ij} + \delta_i + \varepsilon_i \qquad i = 1, 2, \ldots, n; \quad j = 1, 2, \ldots, k \tag{11}$$

where y_i represents target variables (L-moment statistics for Parameter Regression Technique or flood quantiles for Quantile Regression Technique), X_{ij} denotes predictor variables, β_j are regression coefficients, δ_i represents model error reflecting structural limitations, and ε_i is sampling error from limited record lengths and inter-site correlation.

The total error variance combines model and sampling errors following [36]:

$$\Lambda_{ij} = Cov\{\varepsilon_i + \delta_i, \varepsilon_j + \delta_j\} = \begin{cases} \sigma_{\varepsilon i}^2 + \sigma_\delta^2, & i = j \\ \sigma_{\varepsilon i}\sigma_{\varepsilon j}\rho_{\varepsilon ij}, & i \neq j \end{cases} \tag{12}$$

where $\sigma_{\varepsilon i}^2$ represents sampling error variance, $\rho_{\varepsilon ij}$ denotes inter-site correlation coefficient, and σ_δ^2 is model error variance (MEV) [40].

This can be expressed in matrix form as:

$$\Lambda\left(\sigma_\delta^2\right) = \sigma_\delta^2 I + \Sigma(\hat{y}) \tag{13}$$

GLS coefficients are estimated using:

$$\hat{\beta} = \left(X^T \Lambda^{-1} X\right)^{-1} X^T \Lambda^{-1} \hat{y} \tag{14}$$

The residual mean square error equation, used to estimate the MEV (σ_δ^2), is obtained by solving [36,37]:

$$\left(\hat{y} - X\hat{\beta}\right)^T \left[\sigma_\delta^2 I + \Sigma(\hat{y})\right]^{-1} \left(\hat{y} - X\hat{\beta}\right) = n - (k+1) \tag{15}$$

2.4.3. Bayesian Generalised Least Squares Regression (BGLS)

BGLS regression extends GLS by incorporating Bayesian principles to account for sampling variability, inter-site correlation, and differences in record lengths across sites. Unlike classical GLS, BGLS explicitly partitions total variance into model error, sampling error, and signal components and provides posterior distributions of all parameters, resulting in more reliable coefficients and uncertainty quantification [12,32,38,40]. The estimation process is based on the posterior distribution, derived using Bayes' theorem [69]:

$$P(Y \mid D) = \frac{P(D \mid Y)\zeta(Y)}{\int P(D \mid Y)\zeta(Y)dY} \tag{16}$$

where $P(Y \mid D)$ represents the posterior distribution of the parameters (Y); P($D \mid Y$) is the likelihood function based on the observed data (D); and $\zeta(Y)$ is the prior distribution.

2.4.4. Derivation of Priors

Following [70], no prior information is available for the regression coefficients. Therefore, an almost non-informative prior is adopted, represented by a multivariate normal distribution with a mean of zero and a large variance. For the MEV (σ_δ^2), an informative prior is used, specifically a one-parameter exponential distribution:

$$f(\sigma_\delta^2) = \frac{1}{\lambda} e^{-\sigma_\delta^2/\lambda}, \text{where } \sigma_\delta^2 > 0 \tag{17}$$

For the regionalisation of LCV and LSK, λ was assigned a value of 24, following the rationale discussed in [70,71]. For the regionalisation of the mean and flood quantiles, λ is based on an informative exponential prior whose mean equals the inverse of the residual error variance estimate obtained from the ordinary least squares (OLS) regression, following the approach of [34].

2.4.5. Estimation of the Error Covariance Matrix—Sampling Error Variance

The sampling covariance matrix of the L-moments (mean, LCV, and LSK) was derived based on the methods of [4,71,72]. For the mean parameter, the sampling error variance for the mean at site i is given by $\sigma_{\varepsilon i}^2 = \sigma_i^2 / n_i$ where σ_i^2 is the population variance and n_i is the record length at site i. The population variance σ_i^2 is approximated using the regional average population variance:

$$q = \frac{1}{M}\sum_{i=1}^{M}\sigma_i^2 \tag{18}$$

where M is the number of sites in the region, and q represents the regional average of the mean parameter. The sampling error variance for the LCV and LSK is calculated using the regional approximation suggested by [70] and [73]:

$$Var(\hat{y}_i) = \frac{n_a}{n_i} Var(\overline{y}|n_a), \text{ where } \overline{y} = \frac{1}{M}\sum_{i=1}^{M}\hat{y}_i \text{ and } n_a = int\left\{\frac{1}{M}\sum_{i=1}^{M} n_i\right\} \tag{19}$$

$$\mathrm{Var}(\overline{y} \mid n_a) = \frac{\sigma_y^2}{n_a} \tag{20}$$

where $\hat{y}_i$ denotes the at-site estimate (for site i) of the statistic of interest; σ_y^2 is the population variance of the statistic y; n_a is the average record length across all sites, rounded to the nearest integer and $Var(\overline{y}|n_a)$ is the sampling variance of the mean statistic ($\overline{y}$), computed as a function of the mean of the statistic of interest (LCV and LSK), for a sample of size n_a.

2.4.6. Estimation of the Sampling Error—Inter-Site Correlation

Following [34], the inter-site correlation coefficients are calculated using the following exponential function.

$$\rho_{ij} = \psi^{\left[\frac{d_{ij}}{\omega d_{ij}+1}\right]} = \exp\left(\left[\frac{d_{ij}}{\omega d_{ij}+1}\right]\ln\Psi\right) \tag{21}$$

where d_{ij} is the distance between station i and j while Ψ and ω are regional parameters estimated from the data.

2.4.7. Regionalisation Approaches: Fixed Regions and the Region of Influence (ROI)

This study compares the performance of fixed regions, based on regional boundaries, with the ROI approach in the context of forming regions in RFFA. The ROI approach uses geographic proximity between sites as the distance metric and aims to minimise the predictive error variance in the regression model (e.g., refs. [43–45,74]. The ROI approach involves iteratively analysing each station by selecting subsets of its nearest neighbours. Starting with the 10 closest stations, the BGLS regression analysis is performed, and the subset size is incrementally increased in each iteration. This process is repeated until all eligible stations are included in the analysis. The initial ROI size was selected to ensure stable execution of the BGLS regression models. For each iteration, the predictive performance of the regression model was evaluated using the MEV. The optimal ROI for a selected station is determined as the configuration with the lowest MEV, representing the minimum predictive error variance among all tested ROI configurations.

2.4.8. Selecting Predictor Variables

The selection of predictor variables in the BGLS regression approach was supported by several statistical measures, including the MEV and its standard error (stMEV), the pseudo coefficient of determination (R^{-2}_{GLS}), the Average Variance of Prediction (AVP), the Akaike Information Criterion (AIC), and the Bayesian Information Criterion (BIC) [75]. The MEV represents the variance of the unexplained model residuals:

$$\sigma_\delta^2 = \frac{1}{M-k}\left(\left(y - X\hat{\beta}\right)^T \Lambda^{-1}\left(y - X\hat{\beta}\right)\right) \quad (22)$$

The AVP provides a comprehensive measure of predictive uncertainty, with AVPN for new sites and AVPO for existing sites defined by [39] as:

$$AVPN = E\left[\sigma_\delta^2\right] + \frac{1}{M}\sum_{i=1}^{n} x_i Var[\beta|\hat{y}]x_i^T \quad (23)$$

$$AVPO = E[\sigma_\delta^2] + \frac{1}{M}\sum_{i=1}^{n} x_i Var[\beta|\hat{y}]x_i^T - 2\sigma_\delta^2 x_i (X^T\Lambda^{-1}X)^{-1}X^T\Lambda^{-1}e_i \quad (24)$$

where $E\left[\sigma_\delta^2\right]$ represents the expected MEV; $\mathrm{Var}\left[\hat{\beta}\right]$ is the covariance matrix of the regression coefficients given the estimated response $\hat{y}$; x_i is the vector of predictor variables at site i; X is the design matrix containing all predictors, Λ^{-1} is the inverse of the covariance matrix used in the model; e_i represents the unit vector that has 1 at the *i-th* row and 0 in all other rows and M is the total number of sites. AVPO and AVPN are expressed in squared units of the variable.

AIC and BIC are defined as [76,77]:

$$AIC = \frac{SST}{M}\left(1 - \overline{R}^2_{GLS}\right)exp\left(\frac{2(k-1)}{M}\right) \quad (25)$$

$$BIC = \frac{SST}{M}\left(1 - \overline{R}^2_{GLS}\right)M^{\left(\frac{(k-1)}{M}\right)} \quad (26)$$

In this study, both AIC and BIC are calculated following [78] a Bayesian framework. The model with the lowest AIC and BIC values is considered to provide the best balance between fit and complexity. M is the number of sites used in the analysis; SST represents the total squared deviations of observed values from their mean; $\overline{R}^2_{GLS}$ is the pseudo coefficient of determination for the GLS model, accounting for the proportion of explained variability and k is the number of parameters in the model.

The pseudo coefficient of determination ($\overline{R^2}_{GLS}$), introduced by [70], is a modified version of the traditional R-squared (R^2) statistic for use with a GLS regression model. $\overline{R^2}_{GLS}$ accounts for both sampling errors and the MEV, providing a more accurate measure of the model's ability to explain data variability. It ranges from 0 to 1, with larger values indicating a stronger model fit.

The pseudo coefficient of determination is defined as:

$$\hat{R}^2_{GLS} = \frac{n[\hat{\sigma}^2_\delta(0) - \hat{\sigma}^2_\delta(k)]}{n\hat{\sigma}^2_\delta(0)} = 1 - \frac{\hat{\sigma}^2_\delta(k)}{\hat{\sigma}^2_\delta(0)} \quad (27)$$

where $\hat{\sigma}^2_\delta(k)$ and $\hat{\sigma}^2_\delta(0)$ are the MEV when k and no predictor variables are included, respectively. Moreover, the Bayesian Plausibility Value (BPV) (%), introduced by [70] and [39], evaluates the significance of regression coefficients within a Bayesian framework (used at a 5% significance level in this study).

The Standard Error of Prediction (SEP) in Equation (28) quantifies uncertainty in flood quantile and parameter predictions, calculated from the Average Variance of Prediction (AVP) when standardised residuals follow a normal distribution [79].

$$SEP(\%) = 100 \times [\exp(AVP) - 1]^{0.5} \quad (28)$$

Model adequacy is evaluated using GLS standardised residuals—defined as residuals divided by the square root of their variance [74]—to assess GEV parameter and flood quantile estimation performance. Diagnostic evaluation employs QQ-plots of standardised residuals versus Z-scores to assess normality and identify outliers, supplemented by QQ-plots comparing predicted versus observed quantiles to evaluate flood quantile estimation performance for both PRT and QRT approaches in fixed and ROI frameworks.

The present sensitivity analysis focused primarily on prior assumptions within the BGLS framework, while the influence of other modelling choices such as predictor selection, ROI size, inter-site correlation assumptions, and probability distribution choice warrants further investigation in future studies.

2.4.9. Evaluation Statistics

Model validation evaluates PRT-BGLS and QRT-BGLS regression performance with GEV distribution across fixed regions and ROI approaches using leave-one-out (LOO) cross-validation. Each model excludes the target site during calibration, ensuring site-independent predictions. The same LOO validation procedure was applied consistently across all analysed AEPs (50%, 20%, 10%, 5%, 2%, and 1%) and for both the PRT-BGLS and QRT-BGLS frameworks. For the ROI approach, the regional model for each excluded catchment was constructed using the iterative ROI procedure described previously. Catchments exhibiting limited similarity to neighbouring sites were accommodated through progressive expansion of the ROI until the configuration yielding the lowest MEV was identified, ensuring that all catchments could be evaluated under a consistent validation framework. The ROI approach inherently satisfies LOO requirements by treating all sites as ungauged. Performance metrics include median absolute relative error (REr%), mean squared error (MSE), relative root mean square error (RRMSE%), bias (BIAS), and relative bias (rBIAS%), enabling quantitative comparison of regionalisation accuracy for ungauged sites. The evaluation statistics are defined as follows:

$$Median\ REr(\%) = Median\left(\left|\frac{Q_{pred} - Q_{obs}}{Q_{obs}}\right|\right) \times 100 \quad (29)$$

$$MSE = \frac{1}{M}\sum_{i=1}^{M}\left[\left(Q_{pred} - Q_{obs}\right)^2\right] \quad (30)$$

$$\mathrm{RRMSE}(\%) = \left(\frac{\sqrt{\frac{1}{M}\sum_{i=1}^{M}(Q_{\mathrm{pred},i} - Q_{\mathrm{obs},i})^2}}{\mathrm{mean}\ (Q_{\mathrm{obs}})}\right) \times 100 \quad (31)$$

$$BIAS = \frac{1}{M}\sum_{i=1}^{N}\left[\left(Q_{pred} - Q_{obs}\right)\right] \quad (32)$$

$$rBIAS = \frac{1}{M}\sum_{i=1}^{M}\left(\frac{Q_{pred} - Q_{obs}}{Q_{obs}}\right) \quad (33)$$

where Q_{obs} represents observed flood quantiles from at-site GEV frequency analysis using L-moments, Q_{pred} denotes predicted flood quantiles from BGLS regional equations (fixed regions and ROI approaches), and M is the total number of sites in the region.

3. Results

3.1. Selection of Prior Information and Sensitivity Analysis

Following established methodologies, a prior value of λ = 2 was adopted for the mean parameter, reflecting the greater uncertainty and spatial variability associated with mean regionalisation [34]. For LCV and LSK parameters, λ = 24 was selected based on [70], representing a moderately informative prior that provides an appropriate balance between informative and non-informative prior assumptions. Within the BGLS framework, smaller λ values reflect greater uncertainty, whereas larger λ values indicate increased confidence in the prior estimates. Sensitivity analysis evaluated varying prior values from 6 to 84 for LCV and LSK parameters. Results demonstrated minimal sensitivity, with the LSK parameter MEV decreasing marginally from 0.008 at λ = 24 to 0.006 at λ = 84, while AVP decreased by only 5%, indicating negligible impact on the predictive performance. Regression coefficients and derived quantiles exhibited minimal variations across different priors, confirming the robustness and stability of the selected λ = 24 value. This is illustrated in Figure 4, which shows the relationship between the prior λ values and the corresponding AVPO and AVPN values for the LSK parameter. Overall, both the LCV and LSK regionalisation models were relatively insensitive to the selected prior values, with only minor changes observed in MEV, AVP, regression coefficients, and derived flood quantiles across the tested range of λ values. These findings suggest that the regional models are not highly sensitive to reasonable variations in prior specification and remain robust across the tested range of prior values. Similar trends were observed across the analysed flood quantiles.

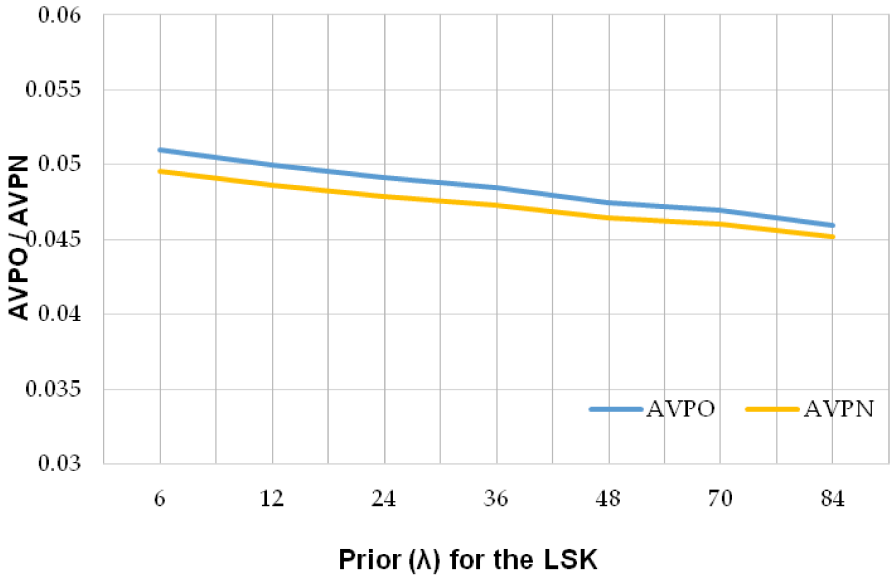


Figure 4. Relationship between the prior (λ) values and the corresponding AVPO and AVPN values for the LSK parameter.

3.2. Parameter Regression Technique (PRT)

3.2.1. PRT-BGLS Fixed Region Analysis

Mean Parameter Regionalisation: Evaluation of 256 predictor combinations identified optimal models based on lowest MEV, highest R^2_{GLS}, and minimal complexity. As shown in Table 2, Figures 5 and 6, combination 213 (*Area*, $I_{6,2}$, *SF*, *SDEN*) achieved optimal performance with MEV of 0.253, R^2_{GLS} of 82.2%, and the lowest AVPO/AVPN values (0.270/0.241). *Area* and $I_{6,2}$ demonstrated essential significance (BPV ≃ 0), while *SF* and *SDEN* showed non-significant contributions. Simpler models like combination 197 (*Area*, $I_{6,2}$, *SDEN*) provided comparable performance with reduced complexity, achieving MEV of 0.250 and R^2_{GLS} of 78.9%.

Table 2. Performance statistics associated with fixed region models for mean flood parameter estimation. (Note: The predictor variables used in this analysis are presented in italics.)

Comb	PVs	MEV	$\overline{R^2}_{GLS}$	AVPO	AVPN	AIC	BIC	BPV%
209	*Area*; $I_{6,2}$; *SF*	0.243	78.6	0.256	0.234	0.278	0.302	0, 0, 11
217	*Area*; $I_{6,2}$; *SF*; *MAE*	0.243	78.6	0.26	0.232	0.284	0.318	0, 0, 14, 48
205	*Area*; $I_{6,2}$; *MAE*; *SDEN*	0.248	79.6	0.265	0.236	0.271	0.304	0, 0, 10, 1.5
199	*Area*; $I_{6,2}$; *SDEN*; *S1085*	0.249	79	0.266	0.238	0.279	0.312	0, 0, 3.1, 26
211	*Area*; $I_{6,2}$; *SF*; *S1085*	0.249	79	0.266	0.238	0.279	0.312	0, 0, 2.2, 14.7
197	*Area*; $I_{6,2}$; *SDEN*	0.25	78.9	0.263	0.241	0.274	0.298	0, 0, 3
213	*Area*; $I_{6,2}$; *SF*; *SDEN*	0.253	82.2	0.27	0.241	0.236	0.265	0, 0, 10, 2.4
198	*Area*; $I_{6,2}$; *SDEN*; *FOREST*	0.253	78.7	0.27	0.241	0.283	0.317	0, 0, 3.7, 59
195	*Area*; $I_{6,2}$; *S1085*	0.267	77.5	0.281	0.257	0.292	0.317	0, 0, 25
201	*Area*; $I_{6,2}$; *MAE*	0.268	77.4	0.282	0.258	0.293	0.319	0, 0, 30
193	*Area*; $I_{6,2}$	0.268	77.4	0.279	0.26	0.287	0.304	0, 0
194	*Area*; $I_{6,2}$; *FOREST*	0.27	77.3	0.285	0.26	0.295	0.321	0, 0, 43
225	*Area*; $I_{6,2}$; *MAR*	0.272	77.1	0.287	0.262	0.297	0.323	0, 0, 59

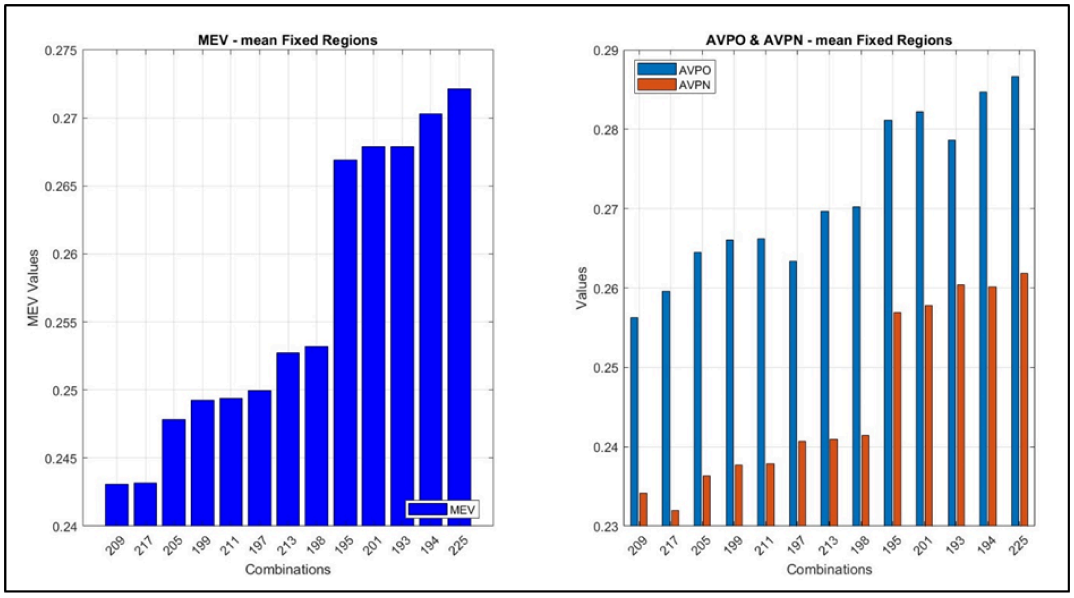


Figure 5. Comparison of performance statistics (MEV, AVPO, AVPN) for the best combinations of predictor variables for the mean flood parameter (fixed region).

LCV Parameter Regionalisation: Among 256 combinations, simple models performed optimally. As seen in Table 3, Figures 7 and 8, combination 65 ($I_{6,2}$ alone) demonstrated superior performance with MEV of 0.0024 and R^2_{GLS} of 34.78%. Enhanced models including combination 66 ($I_{6,2}$, *FOREST*) achieved higher R^2_{GLS} (50.06%) but with non-significant predictor variables (BPV > 5%).

Table 3. Performance statistics associated with fixed region models for LCV parameter estimation.

Comb	PVs	MEV	$\overline{R^2}_{GLS}$	AVPO	AVPN	AIC	BIC	BPV%
65	$I_{6,2}$	0.0024	34.78	0.0077	0.0076	0.0063	0.0064	0, 41
73	$I_{6,2}$; *MAE*	0.0024	47.4	0.01	0.0098	0.0052	0.0055	0, 27, 48
66	$I_{6,2}$; *FOREST*	0.0024	50.06	0.009	0.0088	0.0049	0.0052	0, 55, 36
97	$I_{6,2}$; *MAR*	0.0024	45.93	0.0091	0.009	0.0053	0.0056	0, 95, 42
49	*MAR*; *SF*	0.0024	46.75	0.0088	0.0086	0.0052	0.0055	0, 26, 84
67	$I_{6,2}$; *S1085*	0.0024	37.21	0.009	0.0088	0.0062	0.0065	0, 40, 72
69	$I_{6,2}$; *SDEN*	0.0024	38.33	0.0089	0.0088	0.0061	0.0064	0, 50, 68
81	$I_{6,2}$; *SF*	0.0024	34.58	0.009	0.0088	0.0064	0.0068	0, 41, 95

Note: The predictor variables used in this analysis are presented in italics.

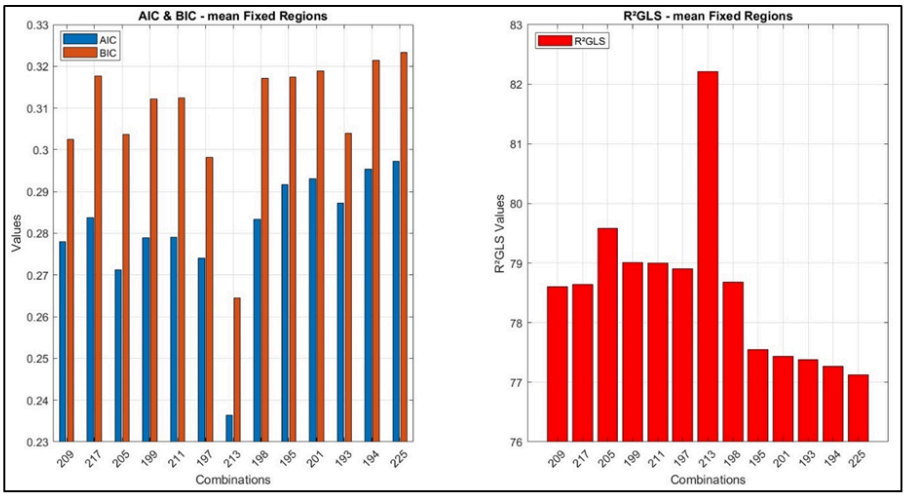


Figure 6. Comparison of performance statistics (AIC, BIC, $\overline{R^2}_{GLS}$) for the best combinations of predictor variables for the mean flood parameter (fixed region).

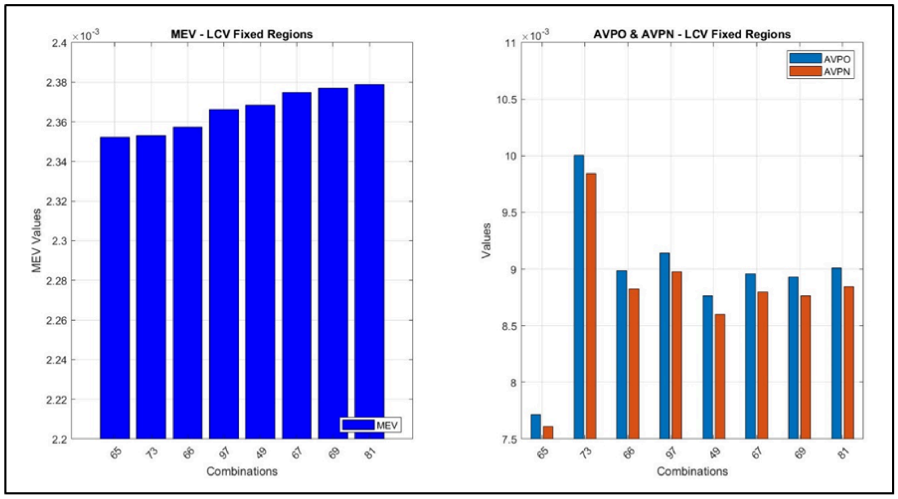


Figure 7. Comparison of performance statistics (MEV, AVPO, AVPN) for the best combinations of predictor variables for the LCV parameter (fixed region).

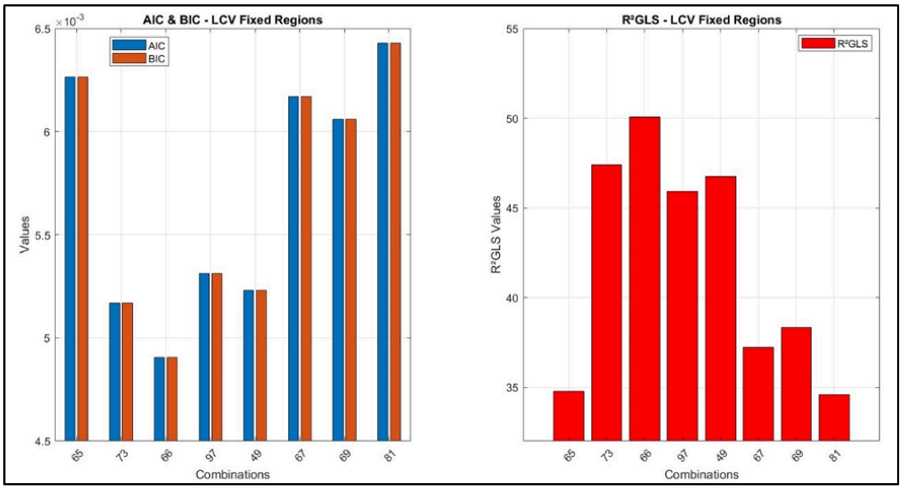


Figure 8. Comparison of performance statistics (AIC, BIC, $\overline{R^2}_{GLS}$) for the best combinations of predictor variables for the LCV parameter (fixed region).LSK Parameter Regionalisation: As with LCV, simple models demonstrated optimal performance for LSK estimation. As shown in Table 4, and in the Appendix A Figures A1 and A2, combination 65 ($I_{6,2}$) showed MEV of 0.0079 and R^2_{GLS} of 25.45%, while combination 1 (constant only) achieved lowest MEV (0.0079) and AVPO (0.0156).

Table 4. Performance statistics of fixed region models for LSK parameter estimation.

Comb	PVs	MEV	$\overline{R^2}_{GLS}$	AVPO	AVPN	AIC	BIC	BPV%
68	$I_{6,2}$; *S1085; FOREST*	0.0081	31.8	0.0319	0.0312	0.012	0.0131	0, 60, 88
1	Constant only	0.0079	0	0.0156	0.0154	0.0165	0.0165	0
66	$I_{6,2}$; *FOREST*	0.008	31.25	0.027	0.0265	0.0119	0.0119	0, 58, 68
81	$I_{6,2}$; *SF*	0.008	25.28	0.027	0.0264	0.0129	0.0136	0, 51, 99
65	$I_{6,2}$	0.0079	25.45	0.0218	0.0215	0.0126	0.0129	0, 51,
67	$I_{6,2}$; *S1085*	0.008	25.26	0.0267	0.0262	0.0129	0.0136	0, 51, 99

Note: The predictor variables used in this analysis are presented in italics.

LOO cross-validation evaluated optimal predictor combinations for mean flood, LCV, and LSK parameters across various AEPs, identifying best-performing models based on statistical accuracy and predictive reliability. The selected models are shown in Table A1 in Appendix A. For the mean flood parameter, combination 213 (*Area*, $I_{6,2}$, *SF*, *SDEN*) achieved superior performance with the lowest MEV (0.224), highest R^2_{GLS} (81.3%), minimal AVPO/AVPN values (0.239/0.214), and lowest AIC/BIC (0.248/0.281). Combination 197 (*Area*, $I_{6,2}$, *SDEN*) demonstrated comparable performance (MEV = 0.247, R^2_{GLS} = 79.3%), while simpler combination 193 (*Area*, $I_{6,2}$) provided acceptable balance between complexity and performance (MEV = 0.251, R^2_{GLS} = 75.6%). For the LCV parameter, combination 65 ($I_{6,2}$) emerged optimally with the lowest MEV (0.0024), acceptable R^2_{GLS} (32.6%), and minimal AVPO/AVPN (0.0078/0.0077). Enhanced models including combination 73 ($I_{6,2}$, *MAE*) improved R^2_{GLS} to 46.3% while maintaining low MEV, and combination 66 ($I_{6,2}$, *FOREST*) achieved R^2_{GLS} of 47.36%. For the LSK parameter, combination 65 ($I_{6,2}$) demonstrated the best performance with lowest MEV (0.008), AVPO (0.0219), AVPN (0.0215), and acceptable R^2_{GLS} (26.18%).

Notably, MEV and AVPO values were significantly higher for mean parameter (MEV: 0.224–0.256, AVPN: 0.214–0.268) compared to LCV (MEV: 0.0024, AVPN: 0.009) and LSK (MEV: 0.008, AVPN: 0.02), highlighting greater regionalisation complexity and uncertainty for the mean parameter relative to dimensionless L-moment ratios.

Flood quantiles for six AEPs (50% to 1%) were predicted using optimal GEV parameter combinations, with evaluation statistics (REr%, RRMSE%) assessing prediction accuracy and reliability. These metrics identified systematic biases, predictive errors, and overall PRT model performance in fixed regions, enabling selection of best-performing predictor combinations for flood estimation across various AEPs. For the LCV parameter, combination 65 ($I_{6,2}$) outperformed combinations 73 and 66, achieving lower prediction errors across all AEPs. REr% values for LCV combination 73 were consistently higher (41.12% for 2% AEP) compared to combination 65 (36.71% for 2% AEP). LSK parameter comparison revealed that combination 65 ($I_{6,2}$) performed better for 50%, 20%, and 10% AEPs, while combination 1 (constant) showed superior results for 5%, 2%, and 1% AEPs.

The optimal fixed region model combined mean flood combination 213 (*Area*, $I_{6,2}$, *SF*, *SDEN*) with LCV ($I_{6,2}$) and AEP-dependent LSK selection: $I_{6,2}$ for 50% AEP and constant for remaining AEPs. This configuration achieved the lowest REr% values: 39.5% (50% AEP), 35.67% (10% AEP), 34.05% (2% AEP), and 34.73% (1% AEP). Alternative mean combinations 199, 197, and 193 provided acceptable performance with reduced complexity, achieving the best RRMSE values (56.4–62.2%). The AEP-dependent LSK selection reflects varying skewness requirements across flood magnitudes, with rainfall intensity becoming critical for extreme events while constant skewness suffices for moderate floods. Table 5 presents the evaluation statistics for the best PRT-BGLS model in the fixed region with LOO cross validation, consisting of the following: mean (*Area*, $I_{6,2}$, *SF*, *SDEN*); LCV ($I_{6,2}$); and LSK ($I_{6,2}$)/(constant).

Table 5. Evaluation statistics for the best PRT-BGLS models in fixed region with LOO validation.

Mean (*Area*; $I_{6,2}$; *SF*; *SDEN*); LCV ($I_{6,2}$); LSK ($I_{6,2}$)—Fixed Region with LOO						
	50% AEP	**20% AEP**	**10% AEP**	**5% AEP**	**2% AEP**	**1% AEP**
Rer%	**39.497**	40.204	36.582	36.153	34.747	34.870
MSE	4935.352	20,317.201	40,856.621	74,691.340	158,224.238	279,034.048
Bias	−7.495	−8.507	−6.624	−3.203	2.108	4.490
RBias	27.205	28.953	30.786	33.308	38.222	43.534
RRMSE%	65.347	61.884	60.180	59.146	58.932	59.716
Mean (*Area*; $I_{6,2}$; *SF*; *SDEN*); LCV ($I_{6,2}$); LSK (constant)—Fixed Region with LOO						
	50% AEP	20% AEP	10% AEP	5% AEP	2% AEP	1% AEP
Rer%	39.880	**40.136**	**35.675**	**35.955**	**34.049**	**34.730**
MSE	4967.756	20,175.907	40,569.801	75,471.685	168,158.973	312,508.169
Bias	−9.863	−12.435	−8.946	−1.137	15.530	32.009
RBias	−9.174	−5.399	−2.664	−0.246	2.301	3.619
RRMSE%	65.561	61.669	59.969	59.455	60.754	63.197

Note: The predictor variables used in this analysis are presented in italics. Bold values indicate the best values for the corresponding evaluation statistic.

3.2.2. PRT-BGLS Region of Influence (ROI)

BGLS regression within the ROI framework was applied to optimal combinations identified from fixed region LOO validation for GEV parameters (mean, LCV, LSK). Four mean combinations were evaluated: 199 (*Area*, $I_{6,2}$, *SDEN*, *S1085*), 213 (*Area*, $I_{6,2}$, *SF*, *SDEN*), 197 (*Area*, $I_{6,2}$, *SDEN*), and 193 (*Area*, $I_{6,2}$). LCV combination 65 ($I_{6,2}$) and LSK combinations 65 ($I_{6,2}$) and 1 (constant) were assessed. Table 6 shows that LCV combination 65 achieved optimal performance with the lowest MEV (0.0026) and reasonable R^2_{GLS} (20.62%). For the LSK parameter, both combinations 65 and 1 achieved the lowest MEV (0.008). Mean parameters 213, 199, and 193 demonstrated similar performances with the best statistics. Eight parameter combinations were evaluated for quantile prediction across various AEPs:

- Mean 193/197/199/213 with LCV 65 and LSK 65
- Mean 193/197/199/213 with LCV 65 and LSK 1

Table 6. Performance statistics for the PRT-BGLS model in ROI.

Parameter	**Comb**	**PVs**	**ROI**	**MEV**	**AVPO**	**AVPN**	$\overline{R^2}_{GLS}$	**AIC**	**BIC**
Mean	193	*Area*; $I_{6,2}$	23	0.1482	0.1825	0.1299	85.4	0.1935	0.2105
	197	***Area*; $I_{6,2}$; *SDEN***	**28**	**0.1637**	**0.2026**	**0.1417**	**86.25**	**0.2185**	**0.2497**
	199	*Area*; $I_{6,2}$; *SDEN*; *S1085*	17	0.1392	0.1969	0.1051	87.38	0.2305	0.2741
	213	*Area*; $I_{6,2}$; *SF*; *SDEN*	19	0.1323	0.1879	0.1038	87.79	0.2193	0.2608
LCV	65	$I_{6,2}$	79	0.0026	0.0082	0.0081	20.62	0.0077	0.0080
LSK	65	$I_{6,2}$	87	0.0080	0.0220	0.0216	20.59	0.0128	0.0132
	1	Constant only	87	0.0080	0.0157	0.0155	0	0.0158	0.0158

Note: Predictor variables are presented in italics. Bold values indicate the best-performing model configuration.

This systematic evaluation identified optimal ROI configurations for each parameter, enabling a comprehensive assessment of prediction accuracy across different complexity levels and AEP ranges.

Evaluation statistics, as shown in Table 7, revealed AEP-dependent optimal model configurations. For 50–5% AEPs, the combination mean (*Area*, $I_{6,2}$, *SDEN*)—LCV ($I_{6,2}$)—LSK (constant) outperformed alternatives, achieving the lowest REr% (33.53–37.60%), RRMSE% (68.62–77.34%), and MSE values. However, for 2–1% AEPs, the combination

mean (*Area*, $I_{6,2}$, *SDEN*)—LCV ($I_{6,2}$)—LSK ($I_{6,2}$) demonstrated superior performance with the lowest REr% (38.61–38.9%), RRMSE% (80.13–82.60%), and MSE values.

Table 7. Evaluation statistics for the best PRT-BGLS models in ROI.

PRT—ROI: Mean (*Area*, $I_{6,2}$, *SDEN*)—LCV($I_{6,2}$)—LSK ($I_{6,2}$)						
AEP	**50% AEP**	**20% AEP**	**10% AEP**	**5% AEP**	**2% AEP**	**1% AEP**
Rer%	35.6188	35.6173	32.3103	37.7965	**38.6143**	**38.8846**
RRMSE	70.8246	72.6767	74.7394	76.9868	80.1339	82.6021
PRT—ROI: Mean (*Area*, $I_{6,2}$, *SDEN*)—LCV($I_{6,2}$)—LSK (constant)						
AEP	**50% AEP**	**20% AEP**	**10% AEP**	**5% AEP**	**2% AEP**	**1% AEP**
Rer%	**33.5288**	**33.6572**	**30.8497**	**37.5943**	42.0137	44.4392
RRMSE	68.6209	70.2911	73.4256	77.3388	83.2891	88.1245

Note: Predictor variables are presented in italics. Bold values indicate the best-performing model configuration.

This AEP-dependent performance reflects increasing skewness variability at extreme flood magnitudes. For higher AEPs (50–5%), skewness remains relatively stable, making constant LSK sufficient without unnecessary complexity. At lower AEPs (2–1%), skewness becomes more variable, necessitating rainfall intensity ($I_{6,2}$) inclusion in LSK modelling. Statistically, extreme flood distributions are increasingly influenced by rainfall intensity as magnitudes increase. Physically, this relationship is logical since extreme floods result from intense rainfall events. Including rainfall intensity in LSK for lower AEPs better captures the heavy rainfall–extreme flooding relationship, improving prediction accuracy. For the mean parameter, SDEN inclusion enhances prediction accuracy by representing efficient runoff collection through higher stream density, leading to larger flood magnitudes.

3.2.3. Comparison Between Fixed Regions and ROI

The optimal fixed region model combined mean (*Area*, $I_{6,2}$, *SF*, *SDEN*), while the ROI framework favoured the simpler mean (*Area*, $I_{6,2}$, *SDEN*), excluding SF. This highlights ROI's ability to select variables suited to local conditions rather than applying uniform predictors across all areas, capturing important regional differences that fixed regions neglect. ROI demonstrated significant advantages for mean parameter models, achieving MEV reductions of 34–41%, highlighting reduced uncertainty. Mean combination 197 (*Area*, $I_{6,2}$, *SDEN*) showed notable MEV reduction from 0.247 (fixed) to 0.164 (ROI), underscoring ROI's effectiveness in minimising predictive uncertainty. ROI achieved SEP reductions of 25–32%, R^2_{GLS} increases of 8–13%, and superior overall performance. Mean combination 197 statistics included reduced AVPO (0.203), AVPN (0.142), AIC (0.218), BIC (0.250), SEP (39%), and R^2_{GLS} of 86%. Similar improvements occurred across other combinations, as summarised in Table A2 in Appendix A.

ROI required fewer sites while maintaining enhanced performance. Mean parameter regionalisation (combination 197) used an average of 28 sites (32% of total), while LCV required 79 sites (90%) and LSK nearly all 88 sites, indicating greater spatial variability for LCV/LSK parameters requiring more stations to reduce sampling uncertainty. RRMSE values were smaller for LCV (9.32%) and LSK (12.16%) compared to the mean parameter (43.62%), reflecting greater heterogeneity and a critical regionalisation role. ROI improvements for LCV/LSK were less pronounced since these models required nearly all sites, making them similar to fixed regions. R^2_{GLS} for LCV decreased from 35% (fixed) to 21% (ROI), confirming minimal differences when full datasets are utilised.

Table 8 compares ROI and fixed-region models using identical parameter combinations across AEPs. ROI demonstrated substantially lower REr% values than the fixed-region approach across most AEPs, indicating improved median prediction accuracy. For example,

REr% decreased from 58.30% to 33.66% at the 20% AEP and from 54.77% to 30.85% at the 10% AEP. RRMSE values were also lower for the ROI model at the more frequent flood events, decreasing from 91.74% to 68.62% at the 50% AEP, from 85.01% to 70.29% at the 20% AEP, and from 80.61% to 73.43% at the 10% AEP. Although RRMSE improvements were not observed across all AEPs, the overall results indicate that the ROI framework provides notable benefits for moderate flood quantiles, while prediction of extreme floods remains subject to greater uncertainty.

Table 8. Comparison of the PRT-BGLS-fixed and PRT-BGLS—ROI using the same combination parameters.

PRT—Fixed: Mean (*Area*, $I_{6,2}$, *SDEN*)—LCV($I_{6,2}$)—LSKB (Constant)						
AEP	**50% AEP**	**20% AEP**	**10% AEP**	**5% AEP**	**2% AEP**	**1% AEP**
Rer%	63.2167	58.2950	54.7720	53.2163	45.6330	43.1578
RRMSE%	91.7361	85.0057	80.6092	76.6406	72.2308	69.7378
PRT—ROI: Mean (*Area*, $I_{6,2}$, *SDEN*)—LCV($I_{6,2}$)—LSKB (constant)						
AEP	**50% AEP**	**20% AEP**	**10% AEP**	**5% AEP**	**2% AEP**	**1% AEP**
Rer%	33.5288	33.6572	30.8497	37.5943	42.0137	44.4392
RRMSE%	68.6209	70.2911	73.4256	77.3388	83.2891	88.1245

Note: Predictor variables are presented in italics.

3.3. Quantile Regression Technique (QRT)

3.3.1. QRTBGLS—Fixed Region

Quantile regression analysis for fixed regions evaluated 256 predictor combinations across quantiles Q_2–Q_{100}. Following PRT selection methodology, optimal combinations included 193 (*Area*, $I_{6,2}$), 194 (*Area*, $I_{6,2}$, *FOREST*), 209 (*Area*, $I_{6,2}$, *SF*), and 225 (*Area*, $I_{6,2}$, *MAR*). Table A3 in Appendix A displays performance statistics for these models. LOO cross-validation revealed combination 193 (*Area*, $I_{6,2}$) as consistently best-performing across all quantiles. BPV values below 0.05 for both predictors confirmed statistical significance. This combination achieved the lowest MEV and predictive variance while maintaining simplicity.

Table 9 demonstrates combination 193's superiority: Q_2 achieved the lowest MEV (0.339) with reasonable R^2_{GLS} (65.6%), while Q_5 and Q_{10} improved to MEV values of 0.330 and 0.312 with corresponding R^2_{GLS} of 73.7% and 73.6%, respectively. Higher quantiles (Q_{20}, Q_{50}, Q_{100}) maintained consistent performance with MEV values of 0.307, 0.315, and 0.343, respectively. Combination 193 emerged as the most reliable model across all quantiles, offering optimal balance between predictive accuracy and simplicity. Its stable low MEV, SEP values, and consistently high R^2_{GLS} across various AEPs established it as the robust choice for regional flood quantile estimation.

Table 9. Performance statistics and evaluation statistics for the best QRT-BGLS models in a fixed region after LOO validation.

Quantiles	**PVs**	**MEV**	**AVPO**	**AVPN**	**SEP%**	$\overline{R^2}_{GLS}$**%**	**AIC**	**BIC**	**Rer%**	**RRMSE**
Q_2	*Area*; $I_{6,2}$	0.339	0.353	0.329	62.460	65.6	0.491	0.526	48.687	90.287
Q_5	*Area*; $I_{6,2}$	0.330	0.343	0.320	61.392	73.7	0.340	0.364	40.120	59.692
Q_{10}	*Area*; $I_{6,2}$	0.312	0.324	0.303	59.483	73.6	0.329	0.352	40.989	59.142
Q_{20}	*Area*; $I_{6,2}$	0.307	0.319	0.298	58.941	73.2	0.324	0.347	41.116	57.751
Q_{50}	*Area*; $I_{6,2}$	0.315	0.327	0.306	59.790	71.8	0.333	0.356	39.666	57.253
Q_{100}	*Area*; $I_{6,2}$	0.343	0.356	0.332	62.787	63.5	0.723	0.773	62.738	93.713

Note: The predictor variables used in this analysis are presented in italics.

3.3.2. QRTBGLS—ROI

The QRTBGLS regression analysis was conducted for the best combination, combination 193 (*Area* and $I_{6,2}$), across various quantiles (Q_2 to Q_{100}) within the ROI framework. A number of evaluation statistics (presented in Table 10) revealed that combination 193 demonstrates good performance across different quantiles, highlighting its reliability for flood quantile prediction.

Table 10. Evaluation statistics for the best QRT-BGLS models in ROI (here ROI is the average number of sites based on the minimum model error variance).

Quantiles	PVs	ROI	MEV	AVPO	AVPN	SEP%	$\overline{R^2}_{GLS}$%	AIC	BIC	Rer%	RRMSE
Q_2	*Area*; $I_{6,2}$	27	0.246	0.290	0.216	49.099	79	0.298	0.325	31.771	69.693
Q_5	*Area*; $I_{6,2}$	32	0.218	0.254	0.196	46.547	81.8	0.260	0.282	38.277	63.958
Q_{10}	*Area*; $I_{6,2}$	33	0.208	0.240	0.189	45.575	82.4	0.246	0.266	39.874	86.092
Q_{20}	*Area*; $I_{6,2}$	33	0.202	0.233	0.184	44.995	82.1	0.240	0.259	34.826	59.235
Q_{50}	*Area*; $I_{6,2}$	33	0.204	0.236	0.186	45.221	82.3	0.244	0.264	35.144	59.455
Q_{100}	*Area*; $I_{6,2}$	33	0.214	0.247	0.194	46.333	80.7	0.294	0.318	39.595	61.573

Note: The predictor variables used in this analysis are presented in italics.

3.3.3. Comparison Between ROI and Fixed

QRT comparison between fixed region and ROI approaches reveals superior ROI performance across all quantiles (Q_2–Q_{100}), evidenced by lower MEV, AVPO, AVPN, AIC, and BIC values (Table A3 and-10). At Q_2, ROI achieved significantly lower MEV (0.246) versus the fixed region (0.339), with similar trends at Q_{100} (0.214 vs. 0.343). ROI demonstrated reduced prediction uncertainty with lower SEP values: Q_2 (49.01 vs. 62.46), Q_{20} (44.99% vs. 58.94%), and Q_{100} (46.33% vs. 62.79%). Higher R^2_{GLS} values confirmed better data fit, with Q_5 achieving 81.8% (ROI) versus 73.7% (fixed region). ROI showed superior evaluation statistics with lower REr% (31.77–39.87%) compared to fixed region (39.66–62.738%). At Q_2, ROI achieved REr% of 31.77% versus 48.69% fixed, while Q_{100} showed 39.6% versus 62.73%. RRMSE values were comparable between methods: fixed region (57.25–93.71%) versus ROI (59.235–86.092%), with ROI improvements at certain quantiles like Q_{100} (61.57% vs. 93.71%).

In fixed regions, PRT outperformed QRT, particularly at lower AEPs. At 50% AEP, PRT achieved REr% of 39.45% and RRMSE% of 65.35% versus QRT's 48.69% and 90.29%. At 2% AEP, PRT maintained lower errors (34.75% REr%, 58.9% RRMSE) versus QRT (39.67%, 57.25%). At 1% AEP, QRT showed notable error increases (62.74% REr%, 93.72% RRMSE) compared to PRT (34.87%, 59.72%). ROI framework improved both models' accuracy, with QRT achieving slight advantages over PRT at lower AEPs. At 50% AEP, QRT achieved 31.77% REr% and 69.69% RRMSE versus PRT's 34% and 69%, respectively. At 1% AEP, QRT achieved 39.6% REr% and 61.5% RRMSE, while PRT showed 39% and 82.6%, respectively, indicating QRT's similar or superior ROI performance.

Figures 9 and 10 illustrate performance differences across frameworks. Fixed region plots (Figure 9) showed reasonable alignment between predicted and observed values, with PRT achieving tighter clustering around the 1:1 line. ROI plots (Figure 10) revealed improved clustering for both models, with QRT showing superior agreement at lower AEPs, reflecting reduced RRMSE values and better regional heterogeneity handling.

QQ-plots of standardised residuals (Figures A3 and A4 in Appendix A) confirmed normality assumptions for both models across frameworks. In fixed regions (Figure A3), PRT exhibited superior performance at higher AEPs, with 100% of residuals within the ±2 range at 50% AEP versus 94.32% for QRT. QRT showed larger tail deviations at lower AEPs, indicating reduced accuracy compared to PRT.

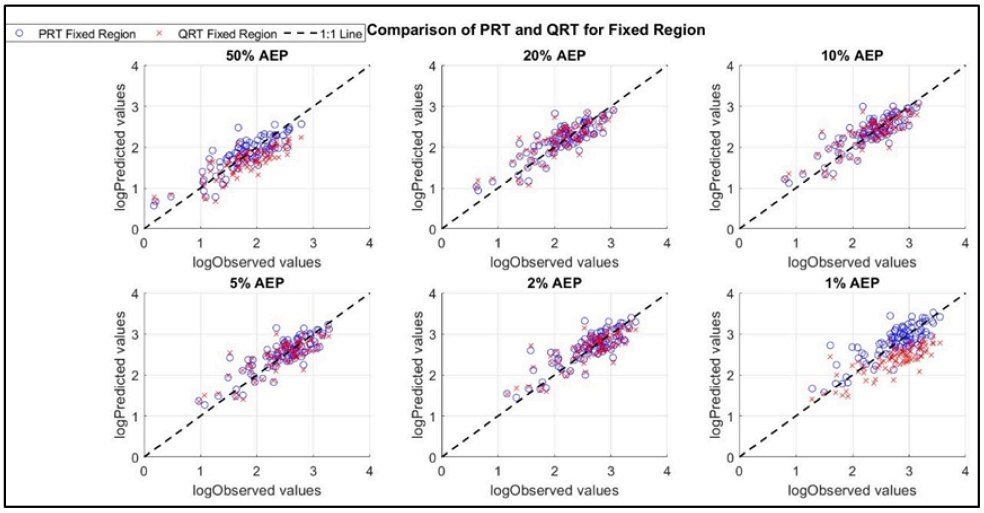


Figure 9. Comparison of Log-Predicted and Log-Observed flood quantiles between PRT and QRT models for a fixed region across AEPs.

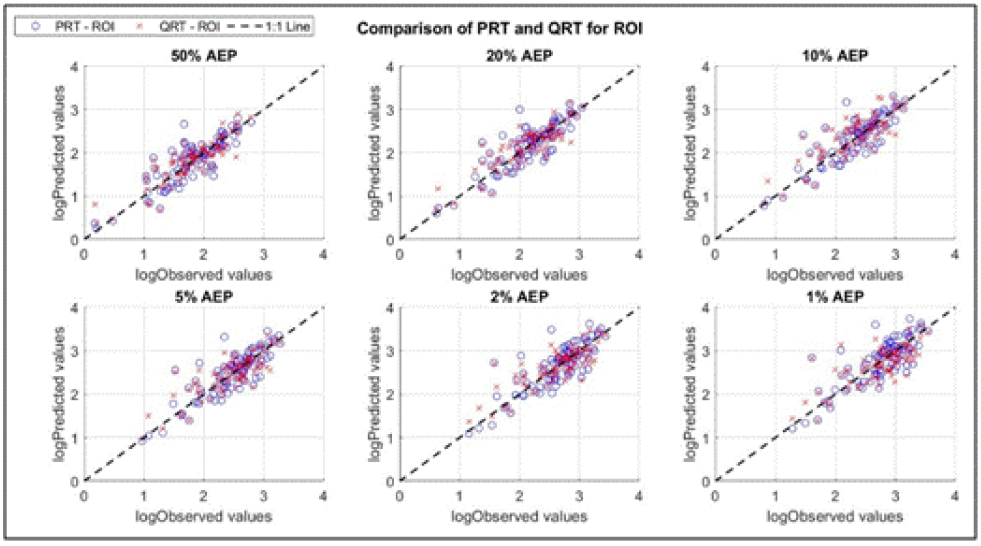


Figure 10. Comparison of Log-Predicted and Log-Observed flood quantiles between PRT and QRT models for ROI across different AEPs.

ROI framework (Figure A4) enhanced both models' performance with stronger theoretical line alignment and higher percentages within ±2 limits. QRT demonstrated slight superiority, particularly at higher AEPs, achieving 100% residuals within limits at 50% AEP versus 96.59% for PRT. At lower AEPs, differences became less significant, but QRT maintained marginally better tail alignment. Overall, ROI enhanced both methods' accuracy, with QRT showing slightly better reliability, particularly for extreme events.

4. Discussion

This study provides a comparative evaluation of PRT-BGLS and QRT-BGLS models within fixed region and ROI frameworks. Across both the PRT-BGLS and QRT-BGLS frameworks, rainfall intensity ($I_{6,2}$) was consistently identified as an important predictor variable and frequently appeared in the best-performing predictor combinations. This highlights the important role of climatic factors in explaining regional flood variability in addition to catchment characteristics. The importance of $I_{6,2}$ is physically reasonable because extreme floods are often caused by intense rainfall events, making rainfall intensity an important factor in flood generation. In fixed regions, PRT outperformed QRT, particularly at lower

AEPs, demonstrating superior robustness. However, ROI generally improved both models' accuracy compared to fixed region approaches, with QRT exhibiting slightly better performance than PRT, particularly for lower AEPs, while maintaining comparable overall predictive performance. The variation in model performance across AEP levels likely reflects the greater uncertainty associated with estimating rare flood events. As AEP decreases, flood quantile estimation becomes increasingly dependent on the upper tail of the fitted GEV distribution, making differences in regionalisation approach and GEV parameter estimation more influential. This may explain the observed changes in model ranking across AEP levels. The larger differences between PRT and QRT at the 1% and 2% AEP levels are likely due to the greater uncertainty associated with rare flood events. At these extreme flood levels, small differences in the estimated GEV parameters can lead to larger differences in the predicted flood quantiles. Therefore, the effect of the regionalisation method becomes more noticeable at lower AEPs.

Although ROI did not reduce RRMSE across all AEPs, it generally produced lower MEV, SEP, AVP, and REr% values, indicating reduced prediction uncertainty and improved overall performance. A similar multi-criteria assessment was adopted by [34], highlighting the importance of evaluating regionalisation performance using multiple statistics rather than a single error measure.

The findings align closely with established literature. Ref. [80] developed regularised linear models for POT-based RFFA in south-eastern Australia using 145 catchments, reporting REr% values of 37–47%, closely matching this study's 31–39% (PRT-ROI) and 32–44% (QRT-ROI). Ref. [81] applied artificial neural networks to 181 catchments, reporting REr% of 33–54%, aligning with QRT-fixed region results (40–63%). Ref. [28] used Fuzzy C-means techniques, reporting REr% of 38–60%, slightly higher than ROI results but closely matching QRT-fixed approaches.

Ref. [82] investigated GAM models across 85 NSW catchments in fixed region and ROI frameworks. For 2% AEP, their fixed region RRMSE was 60%, closely aligned with this study's QRT-fixed (57.3%) and PRT-fixed (58.9%). Their ROI RRMSE (63.6%) compared favourably with QRT-ROI (59.5%) and PRT-ROI (80.1%), supporting BGLS model reliability. Ref. [24] analysed 114 Victorian catchments, finding GAM outperformed QRT for shorter return periods (16–41% median relative error), while QRT excelled at lower AEPs (31–59%), aligning with this study's QRT-fixed results and supporting QRT effectiveness for extreme events. Ref. [83] employed kriging-based RFFA across 558 eastern Australian catchments, reporting 28–36% RE% for NSW, closely matching ROI framework ranges. Ref. [34] used LP3 distribution in BGLS models within fixed region and ROI frameworks, reporting REr% of 35–44% (QRT-fixed), 31–40% (QRT-ROI), 36–46% (PRT-fixed), and 29–36% (PRT-ROI). This study found 40–63% (QRT-fixed), 32–40% (QRT-ROI), 34–40% (PRT-fixed), and 34–39% (PRT-ROI), demonstrating strong agreement. Their RRMSE% values (68–100% QRT-fixed, 53–72% QRT-ROI, 65–90% PRT-fixed, 54–75% PRT-ROI) aligned with this study's findings, confirming the BGLS approach's reliability. Ref. [35] applied ICA-based RFFA to 88 NSW catchments, reporting QRT REr% of 33–44%, closely matching QRT-ROI results. Their PRT model showed 48–59%, slightly higher than this study, suggesting improved PRT performance under the BGLS framework. Ref. [8] compared QRT and PRT using 237 Northeastern US basins, finding QRT slightly outperformed PRT while highlighting PRT's computational simplicity. These findings align with this study, where PRT demonstrated strong fixed region performance while QRT showed superior ROI accuracy.

The results consistently align with previous research, confirming QRT and PRT model reliability in RFFA, with GEV parameters as another outlet for PRT estimation along with LP3 distribution parameters. The findings highlight ROI framework effectiveness in improving predictive accuracy, particularly for QRT, while fixed region approaches confirm PRT

robustness, especially for lower AEPs. These results underscore the importance of selecting appropriate regionalisation techniques to enhance flood quantile estimation performance.

The ROI framework used geographic proximity as the similarity metric and MEV minimisation to identify the optimal neighbourhood configuration. Although ROI consistently outperformed fixed regions, the sensitivity of regionalisation performance to alternative similarity metrics and neighbourhood definitions warrants further investigation.

Although the improvements in REr% and RRMSE% may appear modest, they can reduce uncertainty in design flood estimates and contribute to more reliable flood risk assessment and infrastructure design decisions. Accurate regional flood quantile estimation is important for supporting flood risk management and adaptation strategies. Recent studies have highlighted the role of nature-based solutions and hydrologic control measures, such as retarding basins, in reducing flood risks and enhancing flood resilience [84,85]. Reliable design flood estimates can support the planning, design, and assessment of such flood mitigation measures.

5. Conclusions

This study advances regional flood frequency analysis by examining GEV distribution regionalisation using L-moments within a BGLS framework, evaluating 88 gauged NSW catchments to estimate flood quantiles across various AEPs. The research compares Parameter Regression Technique (PRT) and Quantile Regression Technique (QRT) performance under fixed region and Region of Influence (ROI) approaches using rigorous leave-one-out cross-validation. Key findings demonstrate ROI framework superiority over traditional fixed regions, particularly for mean flood parameter regionalisation, achieving significant MEV and SEP reductions while improving R^2_{GLS} values. This enhanced performance reflects ROI's capacity to address spatial heterogeneity through localised modelling, requiring fewer sites for optimal mean parameter prediction while maintaining competitive performance for L-moment ratios (LCV, LSK) that exhibited minimal framework differences due to their inherently lower spatial variability. Flood quantile estimation revealed important advantages of the ROI framework, particularly through reductions in MEV, SEP, and REr% and improvements in R^2_{GLS} values. Although improvements were not observed consistently across all evaluation measures, particularly RRMSE, the ROI framework generally reduced prediction uncertainty and enhanced overall predictive performance compared with fixed regions. Model comparison showed PRT outperforming QRT in fixed regions, especially at higher AEPs, while ROI implementation generally improved model performance through reductions in MEV, SEP, and REr% values. Notably, QRT demonstrated slight superiority over PRT in the ROI framework, particularly for extreme events (lower AEPs), indicating method-specific responses to localised modelling benefits. These findings suggest that the choice between PRT and QRT may depend on the flood design objective. PRT may be preferable when consistent estimation across multiple AEPs is required, as it regionalises the underlying GEV parameters and preserves the probabilistic structure of the flood frequency distribution. In contrast, QRT may offer advantages when the primary objective is the accurate estimation of specific design flood quantiles, particularly for rarer flood events. However, the differences between the two approaches were generally smaller within the ROI framework, indicating that the choice of regionalisation framework may have a greater influence on predictive performance than the choice between PRT and QRT. The research provides important insights into regional flood estimation and demonstrates the potential of the ROI-BGLS framework for ungauged catchment flood estimation. Although the improvements in REr% and RRMSE% may appear modest, they can reduce uncertainty in design flood estimates and contribute to more reliable flood risk

assessment and infrastructure design. These findings may provide useful insights for future development of Australian Rainfall and Runoff methodologies and similar applications.

The present study used LOO validation to evaluate model performance. Future studies could further validate the proposed models using split-sample testing, independent catchments, and comparison with ARR design equations. Extending the analysis to a larger number of catchments across Australia would also provide further insight into the robustness and transferability of the proposed framework.

Moreover, a limitation of this study is the assumption of stationarity in the AMF series used in the GEV-BGLS framework. Climate change, land-use change, and catchment modifications may introduce non-stationary behaviour in flood records. Therefore, future studies could investigate the application of non-stationary flood frequency analysis within the proposed framework.

Future studies should also integrate advanced uncertainty quantification techniques within BGLS frameworks and investigate additional catchment characteristics and climate variables to further improve predictive performance, ensuring continued advancement in regional flood frequency analysis methodologies. Although FLIKE provides confidence limits for at-site GEV flood quantiles, uncertainty bounds for the regional flood quantile estimates were not explicitly evaluated in this study. Future work could extend the proposed framework by incorporating confidence or credible intervals for regional predictions.

Author Contributions: Data analysis and manuscript drafting: L.R.; conceptualisation, editing, and supervision: A.R., conceptualisation, investigation, editing, and supervision: K.H. All authors have read and agreed to the published version of the manuscript.

Funding: This research received no external funding.

Data Availability Statement: The datasets presented in this article are not readily available because of data limitations. Requests to access the datasets should be directed to Australian Government authorities by paying a prescribed fee.

Acknowledgments: The authors would like to acknowledge the Australian Rainfall and Runoff Revision Project 5 team for providing some of the data. TUFLOW FLIKE was provided freely by the Flike sales team. Streamflow data were obtained from WaterNSW.

Conflicts of Interest: The authors declare no conflicts of interest.

Appendix A

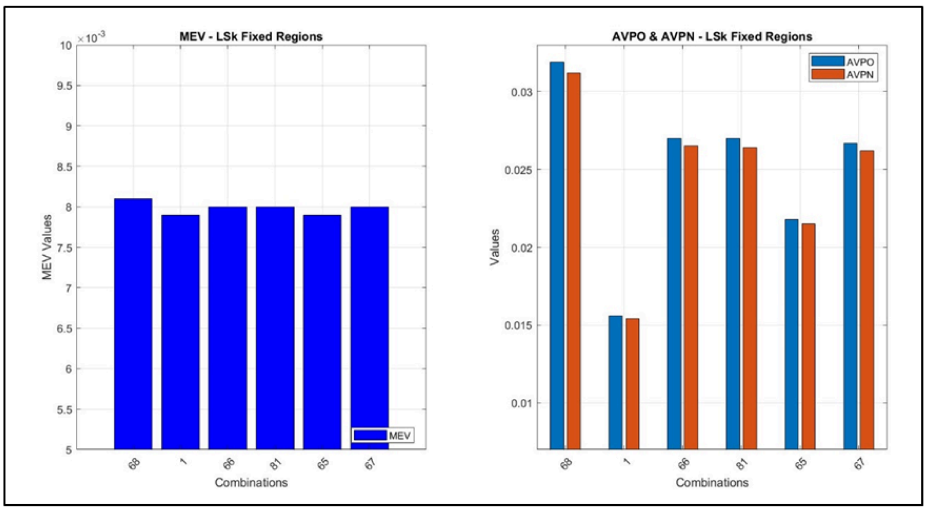


Figure A1. Comparison of performance statistics (MEV, AVPO, AVPN) for the best combinations of predictor variables for the LSK parameter (fixed region).

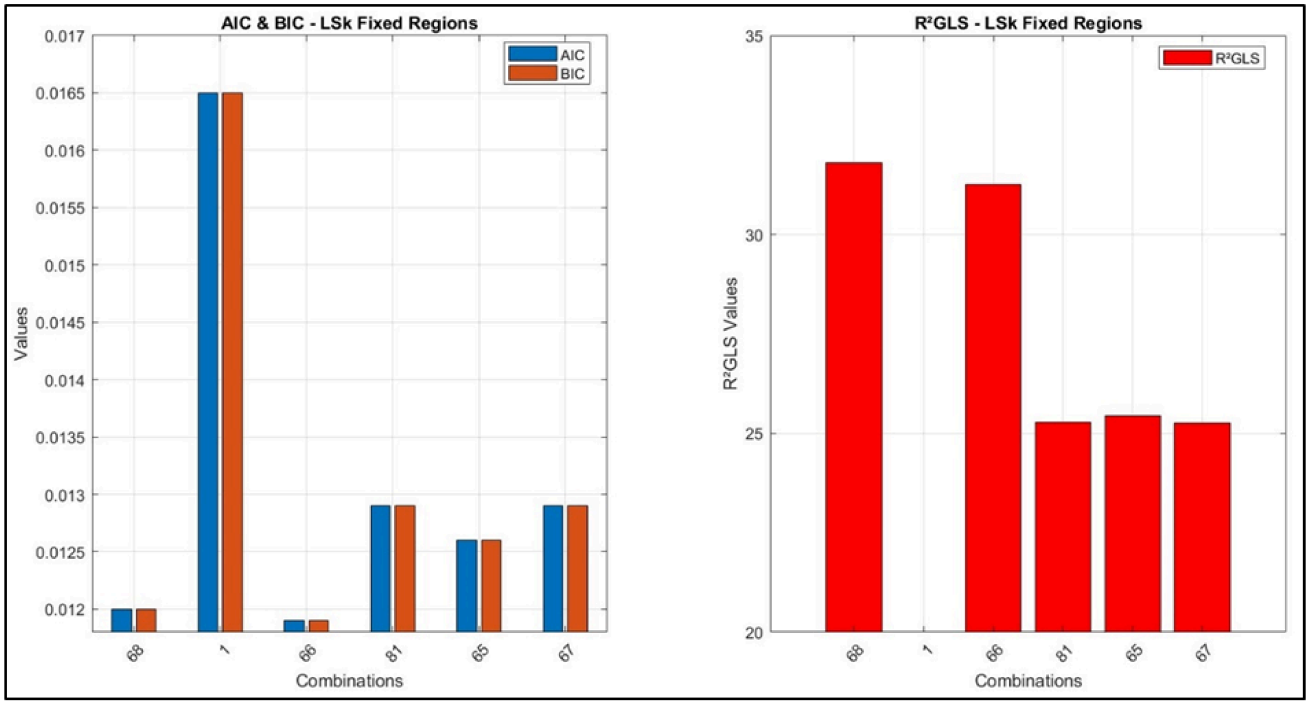


Figure A2. Comparison of performance statistics (AIC, BIC, $\overline{R^2}_{GLS}$) for the best combinations of predictor variables for the LSK parameter (fixed region).

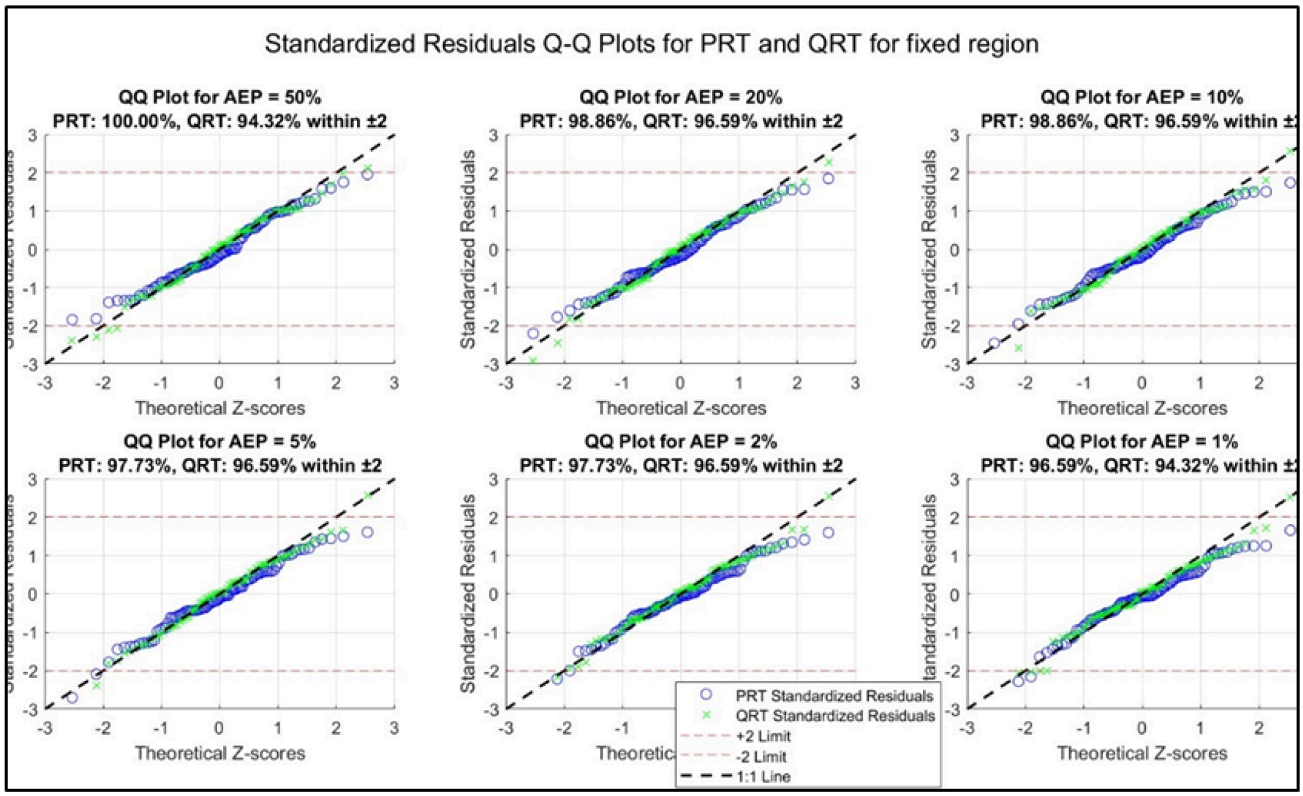


Figure A3. QQ-Plots of standardised residuals vs. theoretical Z-Scores for PRT and QRT Models in fixed region framework across different AEPs.

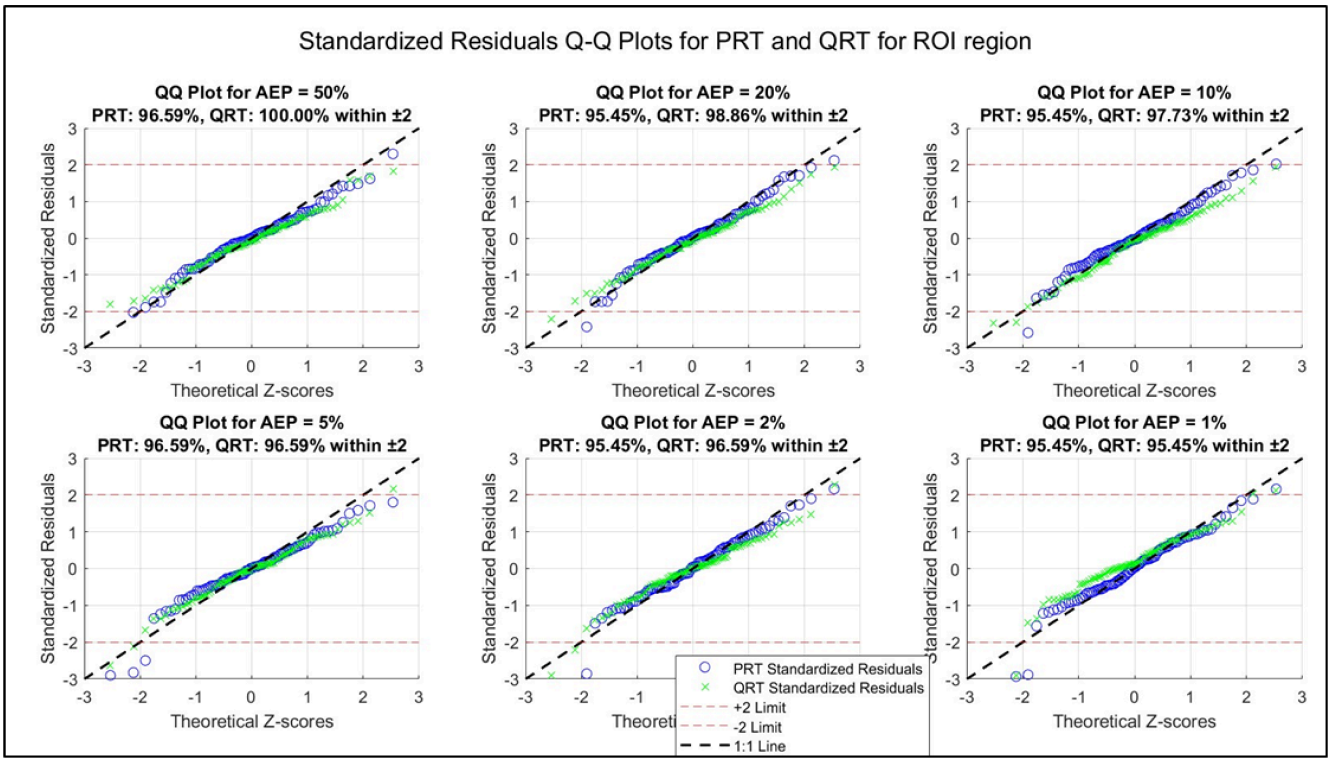


Figure A4. QQ-Plots of standardised residuals vs. theoretical Z-Scores for PRT and QRT Models in ROI framework across different AEPs.

Table A1. Performance statistics of fixed region models for mean flood, LCV and LSK parameter estimation.

Fixed Region—LOO Validation										
Parameter	**Combination (Fixed)**	**PVs**	**MEV**	$\overline{R^2}_{GLS}$	**AVPO**	**AVPN**	**SEP%**	**AIC**	**BIC**	**BPV%**
mean 1	199	*Area*; $I_{6,2}$; *SDEN*; *S1085*	0.229	80.8	0.245	0.219	49.480	0.254	0.288	0, 0, 3.1, 26
mean 2	205	*Area*; $I_{6,2}$; *MAE*; *SDEN*	0.239	79.6	0.255	0.228	50.605	0.265	0.301	0, 0, 10, 1.5
mean 3	217	*Area*; $I_{6,2}$; *SF*; *MAE*	0.244	79.6	0.261	0.233	51.223	0.271	0.307	0, 0, 14, 48
mean 4	197	*Area*; $I_{6,2}$; *SDEN*	0.247	79.3	0.26	0.238	51.837	0.268	0.295	0, 0, 3
mean 5	193	*Area*; $I_{6,2}$	0.251	75.6	0.262	0.244	52.568	0.269	0.288	0, 0
mean 6	194	*Area*; $I_{6,2}$; *FOREST*	0.256	78.6	0.269	0.246	52.811	0.277	0.305	0, 0, 43
mean 7	195	*Area*; $I_{6,2}$; *S1085*	0.26	78.3	0.274	0.25	53.294	0.281	0.31	0, 0, 25
mean 8	201	*Area*; $I_{6,2}$; *MAE*	0.26	78.2	0.274	0.251	53.414	0.282	0.311	0, 0, 30
mean 9	225	*Area*; $I_{6,2}$; *MAR*	0.266	77.8	0.28	0.256	54.014	0.287	0.317	0, 0, 59
mean 10	209	*Area*; $I_{6,2}$; *SF*	0.279	78.1	0.294	0.268	55.439	0.288	0.318	0, 0, 11
mean 11	213	*Area*; $I_{6,2}$; *SF*; *SDEN*	0.224	81.3	0.239	0.214	48.849	0.248	0.281	0, 0, 10, 2.4
LCV 1	73	$I_{6,2}$; *MAE*	0.0024	46.3	0.0101	0.0099	9.973	0.0051	0.0054	0, 29, 48
LCV 2	66	$I_{6,2}$; *FOREST*	0.0024	47.4	0.0067	0.0089	9.444	0.0049	0.0052	57, 38
LCV 3	65	$I_{6,2}$	0.0024	32.7	0.0078	0.0077	8.7649	0.0062	0.0065	43
LSK1	65	$I_{6,2}$	0.0080	26.2	0.0219	0.0215	14.752	0.0120	0.0125	0, 57
LSK2	1	Constant Only	0.0079	0	0.0156	0.0154	12.458	0.0165	0.0165	0

Note: The predictor variables used in this analysis are presented in italics.

Table A2. Comparison of the performance statistics between PRT-BGLS-Fixed region and PRT-BGLS-ROI (here N is the number of stations in the region, ROI is the average number of sites based on the minimum model error variance).

PRT—Fixed										
Parameter	**Combination**	**PVs**	**MEV**	**AVPO**	**AVPN**	**SEP (%)**	$\overline{R^2}_{GLS}$**(%)**	**AIC**	**BIC**	**N**
Mean	193	*Area*; $I_{6,2}$	0.251	0.262	0.244	53	76	0.269	0.288	88
	197	*Area*; $I_{6,2}$; *SDEN*	0.247	0.26	0.238	52	79	0.268	0.295	88
	213	*Area*; $I_{6,2}$; *SF*; *SDEN*	0.224	0.239	0.214	49	81	0.248	0.281	88
LCV	65	$I_{6,2}$	0.002	0.008	0.008	9	35	0.006	0.006	88
LSK	65	$I_{6,2}$	0.008	0.022	0.021	15	25	0.013	0.013	88
	1	Constant only	0.008	0.016	0.015	12	0	0.016	0.016	88
PRT—ROI										
Parameter	**Combination**	**PVs**	**MEV**	**AVPO**	**AVPN**	**SEP %**	$\overline{R^2}_{GLS}$**%**	**AIC**	**BIC**	**ROI**
Mean	193	*Area*; $I_{6,2}$	0.148	0.182	0.130	37	85	0.193	0.210	23
	197	*Area*; $I_{6,2}$; *SDEN*	0.164	0.203	0.142	39	86	0.218	0.250	28
	213	*Area*; $I_{6,2}$; *SF*; *SDEN*	0.132	0.188	0.104	33	88	0.219	0.261	19
LCV	65	$I_{6,2}$	0.003	0.008	0.008	9	21	0.008	0.008	79
LSK	65	$I_{6,2}$	0.008	0.022	0.022	15	21	0.013	0.013	87
	1	Constant only	0.008	0.016	0.015	12	0	0.016	0.016	87

Note: The predictor variables used in this analysis are presented in italics.

Table A3. Performance statistics for the best QRT-BGLS models in fixed region.

Fixed Region—QRT										
	Comb	**PVs**	**MEV**	**stdMEV**	$\overline{R^2}_{GLS}$	**AVPO**	**AVPN**	**SEP%**	**AIC**	**BIC**
Q_2	209	*Area*; $I_{6,2}$; *SF*	0.34	0.131	73.7	0.357	0.326	62.058	0.377	0.410
	194	*Area*; $I_{6,2}$; *FOREST*	0.34	0.135	73.9	0.357	0.326	62.100	0.375	0.408
	225	*Area*; $I_{6,2}$; *MAR*	0.34	0.135	73.9	0.357	0.326	62.094	0.374	0.407
	193	*Area*; $I_{6,2}$	0.34	0.143	74.4	0.353	0.330	62.503	0.358	0.379
Q_5	225	*Area*; $I_{6,2}$; *MAR*	0.342	0.111	72.1	0.359	0.328	62.345	0.379	0.412
	193	*Area*; $I_{6,2}$	0.342	0.106	71.7	0.356	0.332	62.773	0.375	0.396
	194	*Area*; $I_{6,2}$; *FOREST*	0.343	0.106	71.8	0.361	0.329	62.462	0.383	0.417
	209	*Area*; $I_{6,2}$; *SF*	0.350	0.069	71.8	0.368	0.336	63.178	0.383	0.416
Q_{10}	225	*Area*; $I_{6,2}$; *MAR*	0.342	0.110	71.7	0.360	0.329	62.367	0.374	0.407
	194	*Area*; $I_{6,2}$; *FOREST*	0.343	0.106	71.3	0.361	0.329	62.456	0.379	0.412
	193	*Area*; $I_{6,2}$	0.343	0.100	71	0.357	0.333	62.896	0.375	0.396
	209	*Area*; $I_{6,2}$; *SF*	0.346	0.070	71.2	0.364	0.333	62.844	0.380	0.414
Q_{20}	225	*Area*; $I_{6,2}$; *MAR*	0.340	0.125	73.5	0.357	0.326	62.107	0.343	0.374
	194	*Area*; $I_{6,2}$; *FOREST*	0.340	0.123	73.3	0.357	0.326	62.132	0.347	0.377
	193	*Area*; $I_{6,2}$	0.340	0.117	72.3	0.353	0.330	62.545	0.350	0.371
	209	*Area*; $I_{6,2}$; *SF*	0.347	0.086	70.2	0.364	0.333	62.852	0.386	0.420
Q_{50}	209	*Area*; $I_{6,2}$; *SF*	0.339	0.138	76.5	0.356	0.326	62.026	0.301	0.327
	193	*Area*; $I_{6,2}$	0.341	0.149	78.4	0.355	0.331	62.681	0.271	0.287
	225	*Area*; $I_{6,2}$; *MAR*	0.345	0.151	78.3	0.363	0.332	62.726	0.279	0.303
	194	*Area*; $I_{6,2}$; *FOREST*	0.345	0.151	78.3	0.363	0.332	62.741	0.278	0.303
Q_{100}	209	*Area*; $I_{6,2}$; *SF*	0.363	0.155	77.4	0.381	0.348	64.548	0.290	0.316
	193	*Area*; $I_{6,2}$	0.378	0.153	74.5	0.393	0.367	66.588	0.321	0.339
	225	*Area*; $I_{6,2}$; *MAR*	0.387	0.149	72.6	0.407	0.372	67.109	0.353	0.384
	194	*Area*; $I_{6,2}$; *FOREST*	0.389	0.148	72.2	0.409	0.373	67.285	0.358	0.389

Note: The predictor variables used in this analysis are presented in italics.

References

1. Mangukiya, N.K.; Sharma, A. Alternate pathway for regional flood frequency analysis in data-sparse region. *J. Hydrol.* **2024**, *629*, 130635. [CrossRef]
2. Garmdareh, E.; Vafakhah, M.; Eslamian, S.S. Regional flood frequency analysis using support vector regression in arid and semi-arid regions of Iran. *Hydrol. Sci. J.* **2018**, *63*, 426–440. [CrossRef]
3. Durocher, M.; Burn, D.H.; Zadeh, S.M. A nationwide regional flood frequency analysis at ungauged sites using ROI/GLS with copulas and super regions. *J. Hydrol.* **2018**, *567*, 191–202. [CrossRef]
4. Griffis, V.W.; Stedinger, J.R. The use of GLS regression in regional hydrologic analyses. *J. Hydrol.* **2007**, *344*, 82–95. [CrossRef]
5. Ouarda, T.B.M.J. Regional flood frequency modeling. In *Handbook of Applied Hydrology*, 2nd ed.; Singh, V.P., Ed.; McGraw-Hill Education: New York, NY, USA, 2017; Chapter 77.
6. Adhami, M. Regional flood frequency analysis of Northern Iran. *Dokuz Eylül Üniversitesi Mühendislik Fakültesi Fen Ve Mühendislik Derg.* **2024**, *26*, 272–280. [CrossRef]
7. Shu, C.; Ouarda, T.B.M.J. Flood frequency analysis at ungauged sites using artificial neural networks in canonical correlation analysis physiographic space. *Water Resour. Res.* **2007**, *43*, W07438. [CrossRef]
8. Ahn, K.H.; Palmer, R. Regional flood frequency analysis using spatial proximity and basin characteristics: Quantile regression vs. parameter regression technique. *J. Hydrol.* **2016**, *540*, 515–526. [CrossRef]
9. Alshammari, E.; Rahman, A.A.; Ranis, R.; Seri, N.A.; Ahmad, F. Investigation of runoff and flooding in urban areas based on hydrology models: A literature review. *Int. J. Geoinform.* **2024**, *20*, 99–119. [CrossRef]
10. Cunnane, C. Methods and merits of regional flood frequency analysis. *J. Hydrol.* **1988**, *100*, 269–290. [CrossRef]
11. Micevski, T.; Kuczera, G. Combining site and regional flood information using a Bayesian Monte Carlo approach. *Water Resour. Res.* **2009**, *45*, W04405. [CrossRef]
12. Haddad, K.; Rahman, A.; Kuczera, G. Comparison of ordinary and generalised least squares regression models in regional flood frequency analysis: A case study for New South Wales. *Australas. J. Water Resour.* **2011**, *15*, 59–70. [CrossRef]
13. Mulvaney, T.J. On the use of self-registering rain and flood gauges in making observations of the relations of rainfall and flood discharges in a given catchment. *Proc. Inst. Civ. Eng. Irel.* **1851**, *4*, 19–31.
14. Pilgrim, D. *Australian Rainfall and Runoff: Volume One: A Guide to Flood Estimation*; Institution of Engineers Australia: Canberra, Australia, 2001.
15. Institution of Engineers Australia. *Australian Rainfall and Runoff—A Guide to Flood Estimation*; Engineers Australia: Canberra, Australia, 1987.
16. Dalrymple, T. *Flood-Frequency Analyses*; No. 1543; U.S. Government Printing Office: Washington, DC, USA, 1960.
17. Bobée, B.; Mathier, L.; Perron, H.; Trudel, P.; Rasmussen, P.F.; Cavadias, G.; Barbet, M.; Bernier, J. Presentation and review of some methods for regional flood frequency analysis. *J. Hydrol.* **1996**, *186*, 63–84. [CrossRef]
18. Hosking, J.R.M.; Wallis, J.R. Some statistics useful in regional frequency analysis. *Water Resour. Res.* **1993**, *29*, 271–281. [CrossRef]
19. Kjeldsen, T.R.; Rosbjerg, D. Comparison of regional index flood estimation procedures based on the extreme value type I distribution. *Stoch. Environ. Res. Risk Assess.* **2002**, *16*, 358–373. [CrossRef]
20. Zaman, M.; Rahman, A.; Haddad, K. Regional flood frequency analysis in arid regions: A case study for Australia. *J. Hydrol.* **2012**, *475*, 74–83. [CrossRef]
21. Formetta, G.; Prosdocimi, I.; Stewart, E.; Bell, V. Estimating the index flood with continuous hydrological models: An application in Great Britain. *Hydrol. Res.* **2018**, *49*, 123–133.
22. Mosaffaie, J. Comparison of two methods of regional flood frequency analysis by using L-moments. *Water Resour.* **2015**, *42*, 313–321. [CrossRef]
23. Ouarda, T.B.; Charron, C.; Hundecha, Y.; St-Hilaire, A.; Chebana, F. Introduction of the GAM model for regional low-flow frequency analysis at ungauged basins and comparison with commonly used approaches. *Environ. Model. Softw.* **2018**, *109*, 256–271. [CrossRef]
24. Noor, F.; Laz, O.U.; Haddad, K.; Alim, M.A.; Rahman, A. Comparison between quantile regression technique and generalised additive model for regional flood frequency analysis: A case study for Victoria, Australia. *Water* **2022**, *14*, 3627. [CrossRef]
25. Souaissi, Z.; Ouarda, T.B.; St-Hilaire, A.; Ouali, D. Regional frequency analysis of stream temperature at ungauged sites using non-linear canonical correlation analysis and generalized additive models. *Environ. Model. Softw.* **2023**, *163*, 105682. [CrossRef]
26. Chen, M.; Papadikis, K.; Jun, C.; Macdonald, N. Linear, nonlinear, parametric and nonparametric regression models for nonstationary flood frequency analysis. *J. Hydrol.* **2023**, *616*, 128772. [CrossRef]
27. Aziz, K.; Rahman, A.; Shamseldin, A. Development of artificial intelligence based regional flood estimation techniques for Eastern Australia. In *Artificial Neural Network Modelling*; Springer: Cham, Switzerland, 2016; pp. 307–323.
28. Zalnezhad, A.; Rahman, A.; Nasiri, N.; Haddad, K.; Rahman, M.M.; Vafakhah, M.; Samali, B.; Ahamed, F. Artificial intelligence-based regional flood frequency analysis methods: A scoping review. *Water* **2022**, *14*, 2677. [CrossRef]

29. Afrin, S.; Khan, A.Z.; Rahman, M.M. Convolutional neural network (CNN) model for regional flood frequency analysis in southeast Australia. *Nat. Hazards* **2024**, *120*, 11349–11376. [CrossRef]
30. Benson, M.A. *Evolution of Methods for Evaluating the Occurrence of Floods*; Water-Supply Paper; 1580-A; U.S. Geological Survey: Reston, VA, USA, 1962; p. 30.
31. Mantilla, R.; Perez, G.; Velasquez, N.; Wright, D.B.; Yu, G. Regional flood frequency analysis using physics-based hydrologic modeling. *Authorea Prepr.* **2022**. [CrossRef]
32. Haddad, K.; Rahman, A.; Stedinger, J.R. Regional flood frequency analysis using Bayesian generalized least squares: A comparison between quantile and parameter regression techniques. *Hydrol. Process.* **2012**, *26*, 1008–1021.
33. Micevski, T.; Hackelbusch, A.; Haddad, K.; Kuczera, G.; Rahman, A. Regionalisation of the parameters of the log-Pearson 3 distribution: A case study for New South Wales, Australia. *Hydrol. Process.* **2015**, *29*, 250–260.
34. Haddad, K.; Rahman, A. Regional flood frequency analysis in eastern Australia: Bayesian GLS regression-based methods within fixed region and ROI framework—Quantile regression vs. parameter regression technique. *J. Hydrol.* **2012**, *430*, 142–161. [CrossRef]
35. Rahman, A.S.; Khan, Z.; Rahman, A. Application of independent component analysis in regional flood frequency analysis: Comparison between quantile regression and parameter regression techniques. *J. Hydrol.* **2020**, *581*, 124372. [CrossRef]
36. Stedinger, J.R.; Tasker, G.D. Regional hydrologic analysis: 1. Ordinary, weighted, and generalised least squares compared. *Water Resour. Res.* **1985**, *21*, 1421–1432.
37. Stedinger, J.R.; Tasker, G.D. Correction to "Regional hydrologic analysis: 1. Ordinary, weighted, and generalized least squares compared". *Water Resour. Res.* **1986**, *22*, 844. [CrossRef]
38. Reis, D.S., Jr.; Stedinger, J.R. Bayesian MCMC flood frequency analysis with historical information. *J. Hydrol.* **2005**, *313*, 97–116. [CrossRef]
39. Gruber, A.M.; Reis, D.S., Jr.; Stedinger, J.R. Models of regional skew based on Bayesian GLS regression. In *World Environmental and Water Resources Congress 2007: Restoring Our Natural Habitat*; ASCE: Reston, VA, USA, 2007; pp. 1–10.
40. Madsen, H.; Mikkelsen, P.S.; Rosbjerg, D.; Harremoës, P. Regional estimation of rainfall intensity-duration-frequency curves using GLS regression of partial duration series statistics. *Water Resour. Res.* **2002**, *38*, 21-1–21-11. [CrossRef]
41. Haddad, K.; Johnson, F.; Rahman, A.; Green, J.; Kuczera, G. Comparing three methods to form regions for design rainfall statistics: Two case studies in Australia. *J. Hydrol.* **2015**, *527*, 62–76. [CrossRef]
42. Acreman, M.C.; Wiltshire, S.E. Identification of regions for regional flood frequency analysis. *Eos* **1987**, *68*, 1262.
43. Burn, D.H. An appraisal of the region of influence approach to flood frequency analysis. *Hydrol. Sci. J.* **1990**, *35*, 149–165. [CrossRef]
44. Burn, D.H. Evaluation of regional flood frequency analysis with a region of influence approach. *Water Resour. Res.* **1990**, *26*, 2257–2265. [CrossRef]
45. Zrinji, Z.; Burn, D.H. Flood frequency analysis for ungauged sites using a region of influence approach. *J. Hydrol.* **1994**, *153*, 1–21. [CrossRef]
46. Eng, K.; Tasker, G.D.; Milly, P.C.D. An analysis of region-of-influence methods for flood regionalisation in the Gulf-Atlantic Rolling Plains. *JAWRA J. Am. Water Resour. Assoc.* **2005**, *41*, 135–143.
47. Merz, R.; Blöschl, G. Flood frequency regionalisation—Spatial proximity vs. catchment attributes. *J. Hydrol.* **2005**, *302*, 283–306. [CrossRef]
48. Kjeldsen, T.R.; Jones, D.A. An exploratory analysis of error components in hydrological regression modeling. *Water Resour. Res.* **2009**, *45*, W02407. [CrossRef]
49. Rahman, A.; Haddad, K.; Kuczera, G.; Weinmann, E. Regional flood methods. In *Australian Rainfall and Runoff: A Guide to Flood Estimation, Book 3: Peak Flow Estimation*; Springer: Berlin/Heidelberg, Germany, 2019; pp. 105–146.
50. Gado, T.A.; Nguyen, V.T.V. Regional estimation of floods for ungauged sites using partial duration series and scaling approach. *J. Hydrol. Eng.* **2016**, *21*, 04016044. [CrossRef]
51. Khan, Z.; Rahman, A.; Karim, F. An assessment of uncertainties in flood frequency estimation using bootstrapping and Monte Carlo simulation. *Hydrology* **2023**, *10*, 18. [CrossRef]
52. Conway, K.M. *Flood Frequency Analysis of Some NSW Coastal Rivers*; The University of New South Wales: Kensington, Australia, 1970.
53. Kopittke, R.A.; Stewart, B.J.; Tickle, K.S. Frequency analysis of flood data in Queensland. In *Hydrological Symposium, Institution of Engineers Australia, National Conference*; Publication No. 76/2; Institution of Engineers Australia: Canberra, Australia, 1976; p. 20.
54. Malekinezhad, H.; Nachtnebel, H.P.; Klik, A. Regionalisation approach for extreme flood analysis using L-moments. *J. Agric. Sci. Technol.* **2011**, *13*, 1183–1196.
55. Komi, K.; Amisigo, B.A.; Diekkrüger, B.; Hountondji, F.C.C. Regional flood frequency analysis in the Volta River Basin, West Africa. *Hydrology* **2016**, *3*, 5. [CrossRef]
56. Mamoon, A.A.; Rahman, A. Selection of the best fit probability distribution in rainfall frequency analysis for Qatar. *Nat. Hazards* **2017**, *86*, 281–296.
57. Green, J.; Xuereb, K.; Johnson, F.; Moore, G.; The, C. The revised intensity-frequency-duration (IFD) design rainfall estimates for Australia—An overview. In Proceedings of the 34th Hydrology and Water Resources Symposium, Sydney, Australia, 19–22 November 2012; pp. 19–22.

58. Hosking, J.R.M. *Regional Frequency Analysis*; Cambridge University Press: Cambridge, UK, 1997.
59. Kyojo, E.A.; Mirau, S.S.; Osima, S.E.; Masanja, V.G. Frequentist and Bayesian approaches in modeling and prediction of extreme rainfall series: A case study from Southern Highlands Region of Tanzania. *Adv. Meteorol.* **2024**, *2024*, 8533930. [CrossRef]
60. Dey, S.; Zahid, S.T.; Dey, S.; Rahaman, K.M.A.; Islam, A.S. Regional flood frequency analysis in northeastern Bangladesh using L-moments for peak discharge estimation at various return periods in ungauged catchments. *Water* **2025**, *17*, 1771. [CrossRef]
61. Kuczera, G. Comprehensive at-site flood frequency analysis using Monte Carlo Bayesian inference. *Water Resour. Res.* **1999**, *35*, 1551–1557. [CrossRef]
62. Kuczera, G.; Franks, S. At-site flood frequency analysis. In *Australian Rainfall and Runoff: A Guide to Flood Estimation*; Commonwealth of Australia (Geoscience Australia): Canberra, Australia, 2016; pp. 5–99.
63. Bates, B.; Evans, J.; Green, J.; Griesser, A.; Jakob, D.; Lau, R.; Lehmann, E.; Leonard, M.; Phatak, A. *Australian Rainfall and Runoff Revision Project 1: Development of Intensity-Frequency-Duration Information Across Australia*; Engineers Australia, Water Engineering: Barton, Australia, 2015.
64. Jenkinson, A.F. The frequency distribution of the annual maximum (or minimum) values of meteorological elements. *Q. J. R. Meteorol. Soc.* **1955**, *81*, 158–171. [CrossRef]
65. Bílková, D. L-moments and TL-moments as an alternative tool of statistical data analysis. *J. Appl. Math. Phys.* **2014**, *2*, 919–929. [CrossRef]
66. Rima, L.; Haddad, K.; Rahman, A. Low-flow identification in flood frequency analysis: A case study for Eastern Australia. *Water* **2024**, *16*, 535. [CrossRef]
67. Cunnane, C. *Statistical Distribution for Flood Frequency Analysis*; WMO Operational Hydrology Report 1989, 33, WMO-No. 718; World Meteorological Organization: Geneva, Switzerland, 1989.
68. Hosking, J.R. L-moments: Analysis and estimation of distributions using linear combinations of order statistics. *J. R. Stat. Soc. Ser. B* **1990**, *52*, 105–124. [CrossRef]
69. Zellner, A. *An Introduction to Bayesian Inference in Econometrics*; Wiley: New York, NY, USA, 1996.
70. Reis, D.S., Jr.; Stedinger, J.R.; Martins, E.S. Bayesian generalized least squares regression with application to log Pearson type 3 regional skew estimation. *Water Resour. Res.* **2005**, *41*, W10419. [CrossRef]
71. Haddad, K.; Rahman, A.; Ling, F. Regional flood frequency analysis method for Tasmania, Australia: A case study on the comparison of fixed region and region-of-influence approaches. *Hydrol. Sci. J.* **2015**, *60*, 2086–2101. [CrossRef]
72. Tasker, G.D.; Stedinger, J.R. An operational GLS model for hydrologic regression. *J. Hydrol.* **1989**, *111*, 361–375. [CrossRef]
73. Madsen, H.; Rosbjerg, D. Generalised least squares and empirical Bayes estimation in regional partial duration series index-flood modeling. *Water Resour. Res.* **1997**, *33*, 771–781. [CrossRef]
74. Tasker, G.D.; Hodge, S.A.; Barks, C.S. Region of influence regression for estimating the 50-year flood at ungaged sites. *JAWRA J. Am. Water Resour. Assoc.* **1996**, *32*, 163–170. [CrossRef]
75. Gelman, A.; Carlin, J.B.; Stern, H.S.; Rubin, D.B. *Bayesian Data Analysis*; Chapman and Hall/CRC: Boca Raton, FL, USA, 1995.
76. Akaike, H. A new look at the statistical model identification. *IEEE Trans. Autom. Control* **1974**, *19*, 716–723. [CrossRef]
77. Schwarz, G. Estimating the dimension of a model. *Ann. Stat.* **1978**, *6*, 461–464. [CrossRef]
78. Greene, W.H. *Econometric Analysis*; Prentice Hall: New Jersey, NJ, USA, 2003.
79. Tasker, G.D.; Eychaner, J.H.; Stedinger, J.R. Application of generalised least squares in regional hydrologic regression analysis. *U.S. Geol. Surv. Water-Supply Pap.* **1986**, *2310*, 107–115.
80. Pan, X.; Yildirim, G.; Rahman, A.; Haddad, K.; Ouarda, T.B. Peaks-over-threshold-based regional flood frequency analysis using regularised linear models. *Water* **2023**, *15*, 3808. [CrossRef]
81. Zalnezhad, A.; Rahman, A.; Nasiri, N.; Vafakhah, M.; Samali, B.; Ahamed, F. Comparing performance of ANN and SVM methods for regional flood frequency analysis in South-East Australia. *Water* **2022**, *14*, 3323. [CrossRef]
82. Rahman, A.; Charron, C.; Ouarda, T.B.; Chebana, F. Development of regional flood frequency analysis techniques using generalized additive models for Australia. *Stoch. Environ. Res. Risk Assess.* **2018**, *32*, 123–139.
83. Ali, S.; Rahman, A. Development of a kriging-based regional flood frequency analysis technique for South-East Australia. *Nat. Hazards* **2022**, *114*, 2739–2765.
84. Supratman, M.; Kusuma, M.S.B.; Cahyono, M.; Kuntoro, A.A. An assessment of nature-based solutions water infrastructure for flood risk reduction in unplanned area. *Civ. Eng. J.* **2025**, *11*, 1827–1855. [CrossRef]
85. Yuwono, N.; Jayadi, R.; Suharyanto, A. A model for the reduction of flood peak discharge (ΔQp) due to the retarding basin. *J. Civ. Eng. Forum* **2015**, *1*, 57–64.

Disclaimer/Publisher's Note: The statements, opinions and data contained in all publications are solely those of the individual author(s) and contributor(s) and not of MDPI and/or the editor(s). MDPI and/or the editor(s) disclaim responsibility for any injury to people or property resulting from any ideas, methods, instructions or products referred to in the content.